Chemical preservation of tail feathers fromAnchiornis huxleyi, a theropod dinosaur from the Tiaojishan Formation (Upper Jurassic, China)
Peer-reviewed author version

Chemical preservation of tail feathers from Anchiornis huxleyi , a theropod dinosaur from the Tiaojishan Formation (Upper Jurassic, China)

Aude Cincotta, Thanh Thuy Nguyen Tu, Julien Colaux, Guy Terwagne, Sylvie Derenne, Pascal Godefroit, Robert Carleer, Christelle Anquetil, Johan yans

Chemical preservation of tail feathers from *Anchiornis huxleyi*, a theropod dinosaur from the

Tiaojishan Formation (Upper Jurassic, China)

Aude Cincotta[1], Thanh Thuy Nguyen Tu[2], Julien L. Colaux[3], Guy Terwagne[4], Sylvie Derenne[2], Pascal Godefroit[5], Robert Carleer[6], Christelle Anquetil[2], and Johan Yans[7]

[1] School of Biological, Earth and Environmental Sciences, University College Cork, Distillery Fields, North Mall, Cork, Ireland T23 N73K; email: aude.cincotta@ucc.ie

[2] Sorbonne Université, CNRS, EPHE, PSL, UMR 7619 Metis, 4 place Jussieu, 75252 Paris cedex 05, France

[3] Synthesis, Irradiation and Analysis of Materials (SIAM), Department of Physics, University of Namur, 61 rue de Bruxelles, 5000 Namur, Belgium.

[4] Laboratoire d'Analyses par Réactions Nucléaires (LARN), Department of Physics, University of Namur, 61 rue de Bruxelles, 5000 Namur, Belgium.

[5] Operational Directorate 'Earth and History of Life', Royal Belgian Institute of Natural Sciences, 29 rue Vautier, 1000 Brussels, Belgium.

[6] Applied and Analytical Chemistry, Institute for Material Research, University of Hasselt, Campus Diepenbeek, Agoralaan Building D, 3590 Diepenbeek.

[7] Institute of Life, Earth and Environment, University of Namur, 61 rue de Bruxelles, 5000 Namur, Belgium.

Abstract: A panel of geochemical techniques is used here to investigate the taphonomy of fossil feathers preserved in association with the skeleton of the Jurassic theropod *Anchiornis huxleyi*. Extant feathers were analysed in parallel to test whether the soft tissues morphologically preserved in the fossil also exhibit a high degree of chemical preservation. Scanning electron microscopy (SEM) and energy dispersive spectroscopy (EDS) indicate that clays and iron oxide pseudomorphs occur in the surrounding sediment and also reveal the preservation of melanosome-like microbodies in the fossil. Carbon gradient along a depth profile and co-occurrence of carbon and sulphur are shown in the fossil by elastic backscattering (EBS) and particle-induced X-ray emission (PIXE), which are promising techniques for the elemental analysis of fossil soft tissues. The molecular composition of modern and fossil soft tissues was assessed from micro-Attenuated Total Reflectance Fourier Transform Infrared spectroscopy (micro-ATR FTIR), solid-state ^{13}C nuclear magnetic resonance (^{13}C CP-MAS NMR) and pyrolysis- gas chromatography-mass spectrometry in the presence of TMAH (TMAH-Py-GC-MS). Results indicate that the proteinaceous material that comprises the modern feathers is not present in the fossil feathers. The latter and the embedding sediment exhibit a highly aliphatic character. However, substantial differences exist between these samples, revealing that the organic matter of the fossil feathers is, at least partially, derived from original constituents of the feathers. Our results suggest that, despite the morphological preservation of *Anchiornis* feathers, original proteins, i.e. keratin, were probably not preserved in the 160-Ma-old feathers.

Key words: *Anchiornis*; fossil feathers; taphonomy; soft tissue preservation; dinosaur.

INTRODUCTION

Preservation of soft-bodied animals – with non-mineralized tissues – is relatively rare, when considering

the whole geological record. Soft parts of organisms are usually lost during the diverse degradation

processes occurring during fossilization. Their constitutive labile organic compounds are usually too

fragile to be preserved, compared to the 'hard' – biomineralized – parts, which are generally better

preserved. However, some important fossil-bearing sites yield not only exquisitely preserved skeletons

but also remains of soft tissues, such as skin, scales, hair or feathers (e.g. Allison and Briggs 1993; Zhu

et al. 2005; Pan *et al*. 2013). Feathers, the epidermal appendages that form the external covering of

modern birds, have been discovered preserved in close association with fossils of theropod dinosaurs in

Konservat-Lagerstätten – localities that are characterized by the unusual quality of the fossils – from the

Upper Jurassic and Lower Cretaceous of China (Hu *et al*. 2009; Xu *et al*. 2012; Xu *et al*. 1999; Xu *et al*.

2009; Chu *et al*. 2016; Godefroit *et al*. 2013) and Germany (Rauhut *et al*. 2012). During the last twenty

years, Liaoning Province, in north-eastern China, has yielded well-preserved vertebrate fossils with soft

parts (e.g. Benton *et al*. 2008; Kellner *et al*. 2010; Li *et al*. 2012). The most striking discoveries were

exquisitely well-preserved feathered theropod dinosaurs, evidencing their relationship with modern

birds. Since the discovery of the Early Cretaceous *Sinosauropteryx prima* in 1996 (Ji and Ji 1996), many

other feathered specimens have been found (Hu *et al*. 2009; Li *et al*. 2012; Xu *et al*. 2012; Xu *et al*.

2015). In the same way, the discovery of one of the most primitive birds, *Archaeopteryx lithographica*,

associated with well-preserved feathers, constitutes a gigantic step in the comprehension of bird – and

feather – evolution (Christiansen and Bonde 2004). Interestingly, elongate filaments interpreted as

primitive feathers were observed in ornithischian – non-theropod – dinosaurs (Mayr *et al*. 2002; Zheng

et al. 2009). Recently, both 'feather-like' structures and scales were discovered together with remains of

3

71   the middle Jurassic neornithischian *Kulindadromeus zabaikalicus* collected in volcanoclastic deposits

72   from Siberia (Godefroit *et al*. 2014; Cincotta *et al*. 2019; Godefroit *et al*. 2020). Recently, a small

73   theropod dinosaur, the scansoriopterygid *Ambopteryx longibrachium* (Wang et al. 2019) from the Upper

74   Jurassic of China, was described with membranous wings instead of feathered ones. This wing

75   configuration was probably lost during evolution in favour of the feathered wing configuration that

76   occurs in modern birds.

77   In a recent study, Zhao *et al*. (2020) observed the structure of experimentally matured feathers and

78   reported the fusion of barbules in the matured feathers. This result has implications in terms of feather

79   taphonomy and evolution, for the absence of barbules in fossil feathers could be due to their fusion

80   during diagenesis instead of their true absence in the specimen. This is unfortunate that no chemical

81   analyses have been performed to better understand how maturation affects the preservation of

82   biomolecules in feathers.

83   Fossil feathers show a wide range of preservation degrees (e.g. Schweitzer 2011; Xing *et al*. 2016). The

84   study of these diversely preserved structures is crucial for a better understanding of the taphonomic

85   processes leading to their preservation. In most cases, feathers and other types of preserved soft-tissues

86   were deposited in calm, low-energy environments (e.g. Kellner and de Almeida Campos 2002). They are

87   found in diverse environmental settings such as shallow-marine (e.g. Martill and Heimhofer 2007;

88   Barthel 1964; Heimhofer and Martill 2007), lacustrine (e.g. Harms 2002; Sullivan *et al*. 2014; Zhou and

89   Wang 2010), or terrestrial (Manning *et al*. 2013). Different modes of preservation occur for ancient soft

90   tissues: carbonaceous films (e.g. Li *et al*. 2010; Lindgren *et al*. 2015), phosphate (Allison and Briggs

91   1993; Briggs *et al*. 1993), pyrite (Briggs *et al*. 1991; Farrell *et al*. 2013; Leng and Yang 2003), clay

92 minerals (Gabbott *et al*. 2001; Martin *et al*. 2004), aluminosilicates (Butterfield *et al*. 2007), or a

93 combination of these (Wilby *et al*. 1996).

94 Feathers are epidermal appendages mainly composed of keratin (Lucas & Stettenheim 1972), which is

95 present as two secondary structures, alpha-helixes and beta-sheets, corresponding to alpha- and beta-

96 keratin, respectively (e.g. Fraser and MacRae 2012). Alpha-keratin plays a hydrophobic role in avoiding

97 water loss, whereas beta-keratin increases skin hardness (Fraser and Parry 1996; Gregg and Rogers

98 1986). According to Lucas and Stettenheim (1972), the amino acid content of keratin in modern bird

99 feathers is rather homogenous in identical parts of a feather (e.g. in rachis of feathers belonging to the

100 same species), although it varies from one species to another. Nonetheless, feather keratin always

101 comprises high amounts of serine, glycine, proline, and lower quantities of valine, leucine, alanine and

102 cysteine (Arai *et al*. 1983, 1986; Gregg & Rogers 1986; Murphy *et al*. 1990; O'Donnell and Inglis 1974;

103 Saravanan and Dhurai 2012a; Staroń *et al*. 2011).

104 The potential of keratin to resist diagenetic processes is still poorly known. Saitta *et al*. (2017)

105 performed decay and maturation experiments of various keratinous structures, whose conclusions

106 suggest that feather keratin would not survive diagenesis. Although the ultrastructure of feather keratin,

107 i.e. fibrils, can be preserved (e.g. Lindgren *et al*. 2015), there is no direct evidence for the preservation of

108 its proteinaceous compounds. Several immunohistological studies have suggested that keratin could be

109 preserved (Schweitzer *et al*. 1999; Moyer *et al*. 2016; Pan *et al*. 2016), although this method remains

110 highly controversial. By contrast, melanin – the natural pigment present in a variety of soft tissues

111 including hair, skin and feathers – is considered to be more resistant to degradation and fossilization

112 processes. Melanin has been unequivocally identified in various types of fossil tissues, such as fish eyes

113   (Lindgren *et al*. 2012), bird feathers (Colleary *et al*. 2015), non-avian dinosaur feathers (Lindgren *et al*.

114   2015), mammal hair (Colleary *et al*. 2015), or frog skin (McNamara *et al*. 2016).

115   Here, we investigate the ultrastructure and chemical composition of fossil feathers of a theropod

116   dinosaur, *Anchiornis huxleyi* (YFGP-T5199), collected from Upper Jurassic deposits of the Tiaojishan

117   Formation (Liaoning Province, China). Previous study of the same specimen focused on the

118   identification of pigment remains (eumelanin), and evidenced the preservation of melanosomes in the

119   feathers (Lindgren *et al*. 2015). We report new and complementary geochemical information about the

120   preservation of macromolecular compounds in the fossil feathers using a range of analytical tools. The

121   surrounding sediment and modern feathers were analysed in parallel to ascribe pristine constituents.

122   Scanning electron microscopy (SEM) and energy dispersive X-ray spectroscopy (EDS) were used to

123   identify and characterize the elemental composition of preserved pigment organelles and the

124   sedimentary matrix. X-ray diffraction (XRD) was used to analyse the mineralogical composition of the

125   samples in an attempt to understand the role of sediment mineralogy in the preservation of soft tissues.

126   Ion beam analysis (IBA), is recognised as a promising archaeometric tool (Jeynes and Colaux 2016) and

127   has recently been successfully applied to human bone analyses (Beck 2014). In this work, Particle-

128   Induced X-ray Emission (PIXE) and Elastic Backscattering Spectrometry (EBS) were used for the first

129   time on fossil soft tissues to get insights into the heavy (PIXE) and light (EBS) in-depth elemental

130   composition of the samples and demonstrate the co-occurrence of sulphur and carbon. This approach is

131   innovative in the study of organic materials. Organic geochemistry techniques, micro-Attenuated Total

132   Reflectance Fourier Transform Infrared Spectroscopy (micro-ATR FTIR), ^{13}C-Nuclear Magnetic

133   Resonance (NMR), Pyrolysis Gas Chromatography-Mass Spectrometry in the presence of TMAH

134 (TMAH-Py-GC-MS), were applied to characterize the functional groups and other biomolecular

135 components present in the studied samples. To our knowledge, the detailed chemical characterization by

136 ^{13}C NMR and Py-GC-MS of fossil feathers from a non-avian dinosaur has not been done elsewhere.

137

138

139 **MATERIAL AND METHODS**

140

141 *Specimen information*

142 The studied specimen, *Anchiornis huxleyi* (YFGP- T5199) (Fig.1), is a basal Avialan (the description of

143 the specimen is available in the Supplementary Information of Lindgren *et al*. 2015: pp. 18-23) that was

144 collected from the Tiaojishan Formation in the Yaolugou locality (Liaoning Province, China), and

145 belongs to the Yizhou Fossil and Geology Park in Liaoning. The Tiaojishan Formation consists of

146 hundreds of meters of alternating sedimentary and volcanic beds (Liu *et al*. 2012; Yang *et al*. 2006;

147 Yuan *et al*. 2005). Absolute dating on a laterally equivalent formation – the Lanqi Formation – indicates

148 an age ranging between 165.0 ± 1.2 Ma and 153.0 ± 2.0 Ma (Chang *et al*. 2009; Zhang *et al*. 2008),

149 which spans the Callovian-Kimmeridgian interval (Middle-Late Jurassic; Gradstein *et al*. 2012). YFGP-

150 T5199 is embedded in thinly laminated carbonate sediments, corresponding to alternation of very thin

151 marl and thicker clay laminae. These sediments were deposited in the context of a lake affected by

152 episodic volcanic eruptions (Nan *et al*. 2012). Recent U-Pb radiochronological analyses on zircons from

153 the Jianchang locality indicate that the Yanliao Biota, that includes *Anchiornis* as well as pterosaurs and

154   eutherian mammals, is Oxfordian in age (Chu *et al*. 2016). The plumage of the specimen studied herein

155   is morphologically preserved as dark brown residues around the skeleton, especially around the tail and

156   the forelimbs, and on the skull.

157   *Sample description*

158   The studied samples consist of fossil feather fragments dissected from the posterior end of the tail (Fig.

159   1, the dark area in the white box, top right) of YFGP- T5199, as well as fragments of the host sediment

160   (Fig. 1, the light area in the white box). To test for possible chemical contamination of the fossil feathers

161   by sediment, the sediment samples were analysed using the same methodology as for the fossil feathers.

162   Two types of sediment samples were studied: (1) 'host' sediment directly in contact with the feathers

163   from the tail (light area in white box on Fig. 1); and (2) 'remote' sediment located > 100 mm from the

164   fossil on the same slab (yellow box bottom left on Fig. 1).

165   *Sample preparation*

166   Two modern brown wing feathers of *Buteo buteo* (buzzard, Aves: Accipitriformes; RBINS collection

167   number: A4011A01; Supplementary Fig. 1) were analysed for comparative purposes. Different parts of

168   the feathers, rachis and barbs, were analysed with IBA. The modern feathers come from a specimen that

169   died naturally and was stored at -18°C at the Royal Belgian Institute of Natural Sciences prior to

170   analysis.

171   Two types of samples were collected on the fossil specimen: millimetre-sized samples for SEM and

172   EDS, as well as centimetre-sized samples for the other analytical approaches. We took 12 millimetre-

173   sized samples (Fig. 1) from different regions of the body of YFGP-T5199 with a sterile scalpel. The

174   samples were mounted on double-sided carbon tape and sputter-coated with gold (Baltec SCD 050).

175   Centimetre-sized fragments of approximately 5 mm² and 2 mm thick, from fossil feathers (white box in

176   Fig. 1) and sediment (yellow box in Fig. 1) were dissected with a sterile scalpel. Samples were cleaned

177   with distilled water without any additional preparation prior to analysis.

178   Several points were analysed with IBA and micro-ATR FTIR on two centimetre-sized fragments

179   containing both fossil feathers and their 'host' sediment, and one fragment of 'remote' sediment

180   (Supplementary Figs. 1B and 2). Other centimetric samples from the same region were collected for

181   NMR and Py-GC-MS (white and yellow boxes on Fig. 1). These samples were crushed and lipids were

182   extracted in order to (1) eliminate potential contaminants related to sample manipulation; and (2)

183   concentrate macromolecular organic matter which mainly corresponds to proteins in modern feathers.

184   Samples were ground to a fine homogeneous powder in an agate mortar. Lipid extraction involved three

185   successive ultrasonications (ten minutes) in 15 ml of dichloromethane/methanol (2:1, v/v), at room

186   temperature and centrifugation at 3500 rpm (ten minutes). The supernatant was removed and the pellet

187   was dried under nitrogen and stored in the dark at 5 °C prior to analysis.

188   *Analytical methods*

189   Samples were imaged under low vacuum with an environmental QUANTA 200 (FEI) scanning electron

190   microscope (at an acceleration voltage ranging from 20 to 30 kV and working distances of 8 to 15 mm).

191   Subsequent semi-quantitative EDS analyses (single point and mapping) were performed using either an

192   environmental QUANTA 200 (acceleration voltage of 30 kV and working distance of 10 mm) or a field-

193   emission JEOL 7500F (acceleration voltage of 15 kV and a working distance of 8 mm).

194   XRD analyses were carried out on both bulk rock and clay mineral with a Philips diffractometer using

195   Cu K_α radiation. A tube voltage of 40 kV and a tube current of 30 mA were used. The goniometer

196   scanned from 3 to 70 degrees 2θ for the bulk rock and from 3 to 30 degrees 2θ for clay minerals. The

197   clay minerals (< 2 μm fraction) were isolated by successive centrifuging after decarbonatation of the

198   crushed rock with HCl 1N. The preparation was mounted on glass slides and treated according to the

199   three following protocols: (1) natural (air-dried); (2) ethylene-glycol solvation; and (3) heated at 490 $^\circ$C

200   for two hours. Clay minerals were identified according to the position of the (001), or (0001), series of

201   basal reflections on the X-ray diffractograms.

202   Elastic Backscattering Spectrometry (EBS) and Particle-Induced X-ray Emission (PIXE) measurements

203   were performed using a 3 MeV proton (^{1}H) beam from the Tandetron linear accelerator ALTAÏS

204   (University of Namur). PIXE is highly sensitive to Na to U elements whereas EBS signals are enhanced

205   for light elements (e.g. C, N and O) due to strong non-Rutherford cross-sections. These two integrative

206   methods, together, can identify almost all elements of the periodic table. The beam spot size was

207   reduced to 0.5 mm in diameter to minimize topographic effects. Backscattered particles were detected

208   using two detectors mounted at scattering angles of 170° and 165°, whereas the emitted X-rays were

209   collected with an Ultra-LEGe (Ultra Low Energy Germanium) detector mounted at 135°. Angles are

210   given relative to the incident beam direction. A selective filter (6 μm of Al) was mounted in front of the

211   Ultra-LEGe detector to lower the strong Si signal and therefore enhance the rather weak S signal

212   observed in the fossil feathers. The modern brown feathers were analysed at two different locations

213   (barb and rachis; Supplementary Figs. 1 and 2).Two locations were analysed in the fossil feathers. The

214   'host' sediment was analyzed at three different locations (at 1.7, 3.2, and 4.8 mm away from the fossil)

215   and the 'remote' sediment at one location (Supplementary Fig.2). All the samples were analysed using

216   the same experimental settings. A certified reference material (BCR-126A lead glass from NIST) was

217   analysed to (1) calibrate the detectors (both EBS and PIXE); and (2) estimate the accuracy of the PIXE

218   measurements. The EBS spectra were analysed with DataFurnace software (Jeynes *et al*. 2003) together

219   with the cross-sections generated by SigmaCalc (Gurbich 2016) to derive the depth profiles of the major

220   elements (see Supplementary Fig. 4 for carbon). The integral of C, O and Si depth profiles (integration

221   limits set to 0 – 25 000 TFU[1], or 0 – 3 µm considering a density of 2.65 g/cm³) yields the C, O and Si

222   equivalent thicknesses given in TFU (details on the global uncertainty calculations can be found in

223   Supplementary Table 1). The PIXE spectra were manipulated with GUPIX software (Campbell *et al*.

224   2010). The matrix composition to be used in GUPIX was determined by integrating the depth profiles of

225   the main components observed by EBS (i.e. C, O and Si) on a given interval (0 – 100 000 TFU).

226

227   Micro-Attenuated Total Reflectance Fourier Transform Infrared spectroscopy (micro-ATR FTIR) was

228   performed on modern and fossil feathers using a Bruker Vertex 70 FTIR spectrometer (University of

229   Hasselt, Belgium) equipped with a Hyperion 2000 microscope and MCT detector. The infrared spectra

230   were collected in the mid-IR range, from 4000 to 600 cm^{-1}, and 32 scans were acquired in Attenuated

231   Total Reflectance (ATR) mode (Ge –ATR crystal) with a resolution of 4 cm^{-1}. FTIR spectroscopy was

232   used on a modern buzzard feather (dark regions), one sample of fossil feather from the tail of *A. huxleyi*

233   and the surrounding sediment, to identify the presence or absence of functional groups in their molecular

234   composition.

235   [13]C Nuclear Magnetic Resonance is a spectroscopic method that documents the chemical environment of

236   carbon in organic compounds. Solid state ^{13}C NMR spectra of the lipid-free samples were obtained at

237   125 MHz (Bruker Avance 500 spectrometer) using a 4 mm zirconium rotor, with a cross-polarization

238   (CP) sequence and magic angle spinning (MAS) at 14 kHz. CP-MAS ^{13}C NMR spectra were acquired

239   with contact time of 1 ms and recycle time of 1s (fossil and sediment) or 3s (modern feathers). The use

240   of a single contact time does not allow precise quantification of the identified chemical functional

241   groups. Each spectrum was the result of 6 000 (modern samples) to 400 000 (sediments) scans.

242

243   Curie point Pyrolysis-Gas Chromatography- Mass Spectrometry (Py-GC-MS) gives insight into the

244   molecular composition of organic macromolecular materials through their thermal degradation into

245   molecular building blocks that can be separated by gas chromatography (GC) and further identified by

246   mass spectrometry (MS). Tetramethylammonium hydroxide (TMAH) was used to enhance the thermal

247   breakdown of macromolecules and induce *in situ* methylation of pyrolysis products, which, in turn,

248   enhance their detection and identification in GC-MS. The samples were mixed with an excess of TMAH

249   (25 wt % in methanol) in a 1:1 (wt/wt) ratio before loading in ferromagnetic tubes with Curie

250   temperature of 650 °C. Two mg were used for the modern samples, 6 mg for the fossil feathers, and 16

251   mg for the sediment. Curie point pyrolysis was carried out with a Pilodist Curie flash pyrolyser. Samples

252   were heated at their Curie temperature for 10 s under a He flow of 1 ml/min. The instrument was

253   coupled directly to a GC-MS system. The pyrolysis products were separated using a Trace Thermo gas

254   chromatograph equipped with a Rxi5SilMS column (30 m × 0.25 mm i. d., 0.5 μm film thickness).

255   Helium was used as carrier gas at constant pressure of 15 psi. The injector temperature was 280 °C in

256   spitless mode. The oven temperature was maintained at 50 °C for ten minutes and was progressively

257   increased to 310 °C at 2 °C/min. Coupled to the gas chromatograph was a DSQ Thermo mass

258 spectrometer with a heated interface (310 °C), electron energy of 70 eV and ion source at 220 °C,

259 scanning from m/z 35 to 800 at 2 scans/s. Compounds were assigned on the basis of their mass spectra,

260 comparison with the NIST library mass spectra, published mass spectra (e.g. Gallois *et al*. 2007;

261 Templier *et al*. 2013) and GC retention times. The molecular structure of all compounds present in

262 substantial amount was investigated without any ion selection that could have biased interpretations.

263 *Institutional Abbreviation*

264 YFGP: Yizhou Fossil and Geology Park; RBINS: Royal Belgian Institute of Natural Sciences; NIST:

265 National Institute of Standards and Technology.

266

267 **RESULTS**
268

269 *SEM/EDS and XRD*

270 SEM of the fossil feathers revealed that they are embedded in a sedimentary matrix containing mainly

271 quartz, carbonates, and phyllosilicates. The latter are organized in thin platelets oriented parallel to each

272 other (Figs. 2A-B). A feather sample from the right wing of *Anchiornis* (sample 1 on Fig. 1) showed

273 abundant rounded crystals that are present only beneath the surface. They occur mainly as framboids

274 (Fig. 2C), but also as individual microcrystallites (Fig. 2D) and, in some cases, are associated with

275 voids. Framboids are spheroidal or ovoid, 6 to 9 μm in diameter and contain dozens of euhedral crystals,

276 750 nm in diameter. In contrast, individual cubic crystals are much smaller (about 500 nm³) and contain

277 micro-crystallites (Fig. 2D). EDS analyses indicate that the sediment is composed of Fe, Si, O, Al, C, Ca

278   (and Mn, K, Mg), probably indicating the presence of quartz, calcite, and various phyllosilicates. XRD

279   analyses confirmed the presence of these minerals in the sediment (Fig. 3A). In addition, the XRD

280   spectrum of the < 2 μm phase shows that expansive material, such as illite and interstratified

281   illite/smectite, is present in the sediment (Fig. 3B). Due to their characteristic framboidal shape and

282   elemental composition, the crystal clusters observed beneath the fossil feather surface are attributed to

283   diagenetic iron oxides or hydroxides. Indeed, although the framboidal habit is common for iron

284   sulphides, the lack of sulphur here shows they are rather iron oxide pseudomorphs probably resulting

285   from the *in situ* weathering of pyrite framboids (Blanco *et al*. 2013; Kaye *et al*. 2008; Nordstrom 1982;

286   Wang *et al*. 2012). These structures are associated with thin clay overgrowths (arrow in Figs. 2C, E),

287   indicating that the iron oxides (or the preceding pyrites) precipitated first. Tiny stellate minerals were

288   also observed and identified as probable iron oxides by X-ray spectroscopy (Fig. 2F). The presence of

289   calcium carbonates, feldspars (Fig. 2G) and quartz (Fig. 2H) in the sedimentary matrix was confirmed

290   by X-ray spectroscopy.

291   Elongate microbodies, 650 to 950 μm, and their associated imprints were observed in three samples (6,

292   9, and 12, on Fig. 1) collected from the anterior and posterior parts of the dinosaur tail (Fig. 4).

293   Microbody imprints are abundant, tightly packed together and randomly oriented (Figs. 4A–B). They

294   likely represent traces of melanosomes. Similar microbodies interpreted as melanosomes have

295   previously been observed in feathers from the crest of this specimen (YFGP-T5199; Lindgren *et al*.

296   2015). Here, isolated elongate structures were observed (Fig. 4C). These fossil organelles are preserved

297   within the thin clay-rich sediment.

298

14

Ion Beam Analysis (IBA): EBS and PIXE

300 The great virtue of EBS is to be capable of yielding the elemental depth profiles non-destructively from

301 the outermost microns of the sample with good sensitivity and depth resolution (Jeynes and Colaux

302 2016). A typical EBS spectrum obtained from the fossil feathers is shown in Supplementary Figure 3

303 together with its best fit. The experimental spectrum was inverted to recover the elemental depth profiles

304 (examples are shown for carbon in Supplementary Fig. 4). Integration of these elemental depth profiles

305 allows derivation of the concentration of each element at a given depth. Figure 5A clearly shows that the

306 carbon enrichment in the near surface region (ca. 60%) decreases at increasing distance from the fossil

307 feathers, reaching a minimum in the 'remote' sediment (ca. 14%). Sample concentrations of oxygen and

308 silicon (although less obvious) follow an opposite trend. The nitrogen content in the modern buzzard

309 feathers is ca. 20-26 %. The very low content of nitrogen in the fossil (ca. 5%) and even less (under the

310 limit of detection) in the remote sediment (Supplementary Fig.3) precluded its depth profiling.

311 In contrast, EBS analysis of modern buzzard feathers shows homogeneous concentrations with depth

312 (Supplementary Fig. 5). Carbon content in the buzzard feathers is about 60 at. %, while nitrogen and

313 oxygen are both around 20 at. % for the rachis and around 25 and 15 at. % respectively for the barbs.

314 Typical PIXE spectra acquired from the fossil feathers, 'host' sediment and 'remote' sediment are

315 shown in Figure 5B. The samples differ in the amounts of several elements present (Supplementary

316 Tables 1–2). Of particular interest is the sulphur content: there are elevated concentrations of sulphur in

317 the fossil feathers (average $1,842 \pm 208.5$ ppm), less in the 'host' sediment ($1,162 \pm 143$ ppm), and much

318 lower concentrations in the 'remote' sediment (98 ± 35 ppm). The concentration of S in the fossil

319 feathers is roughly twenty times lower (ca. 0.2 wt. %) than in the modern bird feathers (ca. 3.7 – 4.3 wt.

320 %). The co-occurrence between sulphur and carbon is also highlighted (Table 1). Both concentrations

321 decrease with depth within the fossil feathers whereas the reverse situation is observed for Si and O.

322

323 *^{13}C NMR*

324 The ^{13}C NMR spectrum of buzzard feathers (Fig. 6A) shows a complex signal in the aliphatic region,

325 with well-resolved peaks between 10 and 65 ppm and a narrow peak at 173 ppm, due to carboxyl

326 carbons, i.e. carboxylic groups and esters and amides. Two additional, less intense, signals can be seen

327 at 129 ppm and 158 ppm in the unsaturated/aromatic carbon region. In comparison to the spectrum of

328 modern feathers, the ^{13}C NMR spectra of the fossil feathers and their surrounding sediment show much

329 simpler patterns (Figs. 6B–C). The spectra are similar to each other and both are dominated by a broad

330 peak in the aliphatic region, maximizing at 30 ppm and thus indicative of long alkyl chains. Two

331 additional broad signals contribute to the spectra. The first one occurs as a broad shoulder between 68

332 and 80 ppm, in the O-alkyl C and N-alkyl C range, and the second one is a broad peak at 129 ppm,

333 attributed to aromatic carbons.

334

335 *Micro-ATR FTIR spectroscopy*

336 The micro-ATR FTIR spectra of the theropod feathers, the embedding sediment and the modern buzzard

337 feather (dark regions) are shown in figure 7.

338 The spectrum of the dark region of a modern buzzard feather shows characteristic bands of secondary

339 amides – as in proteins and polypeptides – at 1628 cm^{-1} (C=O stretch of Amide I), 1531 cm^{-1} (C-N

340 stretch, Amide II) and 1239 cm^{-1} (N-H in plane bending coupled with C-N stretch, Amide III). Broad

16

341 bands around 3274 and 3125 cm^{-1} can be attributed to the N-H stretching of secondary amides. The

342 bands at 2961, 2922 and 2852 cm^{-1} are assigned to the C-H stretching of methylene and methyl groups.

343 These two spectra are very similar and no significant differences could be found between IR response of

344 the dark and white regions of the same feather.

345 The spectrum of the fossil feathers has a different pattern but some similarities with the modern buzzard

346 feather appear. The distinct bands at 2920 and 2851 cm^{-1} can also be attributed to C-H stretching of

347 methylene and methyl groups. These associated bands are also present in the IR spectrum of the

348 surrounding matrix but with different relative intensities. A broad region around 3300 cm^{-1} is present,

349 although much less marked, and is indicative for O-H stretching as found in carboxylic groups and

350 alcohols. In the spectra of the fossil feathers, a broad band at about 1560 cm^{-1} can be attributed to

351 carboxylate. This band is not present in IR spectrum of the sediment. Another broad band around 1412

352 cm^{-1} is found in the spectrum of the fossil feathers and might be related to the presence of CaCO$_3$ in

353 overlap with C-H bending vibrations at 1460 and 1380 cm^{-1} (Andersen and Brečevic 1991; Kroner et al.

354 2010; Kiros et al. 2013) . This is also confirmed by the presence of weak bands at 873 and 718 cm^{-1}. The

355 IR spectrum of the sediment shows a similar, but less defined, absorption band between 1415 and 1463

356 cm^{-1}. The IR spectrum of the fossil feathers and its surrounding matrix both show a narrow band at 1260

357 cm^{-1} that could be attributed to the Si-CH$_3$ vibrations. Both spectra show an intense broad band at 1013

358 cm^{-1} together with the weaker bands at 873 and 797 cm^{-1} related to the sedimentary matrix (clay

359 minerals, quartz, silicates, Si-O stretching). The IR spectrum of the sedimentary matrix shows an

360 additional band at 720 cm^{-1} that is also present, although very weak, in the fossil, indicating long-chain

361 alkyl groups (CH$_2$ rocking vibrations). All the peaks mentioned above are absent in the IR spectra of the

362 modern feather.

17

363

TMAH Py-GC-MS

Pyrochromatograms were obtained for the three following samples: the modern and fossil feathers, and

the 'host' sediment. In agreement with previous studies on bird feathers (Brebu and Spiridon 2011;

Saitta *et al*. 2017), the pyrochromatogram of the modern feathers is dominated by cyclic molecules

containing nitrogen, along with methylbenzene **1**, methylbutane nitriles **2, 3** and cyclohexanedione **11**

derivatives (Fig. 8A). Detailed interpretation of mass spectral fragmentation patterns allowed

identification of the major pyrolysis products (Table 2) and further assignment to possible source.

Molecular structures are given in Appendix, with methyl groups added by TMAH indicated in bold.

Products **6**, **8**, **10** result from direct methylation of alanine, valine and proline, thus pointing to a

proteinaceous origin for the feathers. This is further supported by the occurrence in substantial amounts

of alkylnitriles **2**, **3** resulting from dehydration of amides involving isoleucine and leucine, respectively,

and of methoxybenzenes **7**, **9** released through homolysis of the side chain of tyrosine (Ratcliff *et al*.,

1974). Methylbenzene **1**, pyrrole **4** and ethylbenzene **5** are rather ubiquitous pyrolysis products in

sedimentary organic matter. However, they can also be released upon pyrolysis of phenylalanine and

serine (Gallois *et al*. 2007). Mass spectral fragmentation pattern (base peak at m/z 82) suggests an origin

from the side chain of histidine for compound **16**. Similarly, compound **17** probably corresponds to a

valine derivative as its mass spectrum is characterized by the loss of 42 amu (i.e. valine side chain).

Dimethylcyclohexanedione **11** was reported as pyrolysis product of glycine (Moldoveanu 2009).

Glycine is also present as its diketopiperazine **15** resulting from combined dehydration and cyclisation

(Simmonds *et al*. 1972). The same mechanism involving two different amino acids (isoleucine-glycine)

18

384   leads to another diketopiperazine **18** (Hendricker and Voorhees 1996). The formation of more complex

385   diketopiperazines was proposed by Templier *et al*. (2013) from tripeptide units. Similar mechanism can

386   be invoked for the formation of compound **19** from valine, as well as compounds **20** and **21** from serine

387   and leucine (Table 2; Supplementary Fig. 6). Imidazolidinedione **12** probably results from the internal

388   cyclisation of tripeptide comprising an alanine unit as reported by Templier et al. (2013; Supplementary

389   Fig. 6). The formation of imidazolidinone **13** can be related to the decomposition of bicyclic amidine

390   derived from valine as suggested by Basiuk and Navarro-González (1997; Supplementary Fig. 6).

391   Another decomposition pathway of bicyclic amidine is probably responsible for the formation of

392   imidazolidinone **14** from valine and possibly glycine (Templier *et al*. 2013). As far as we know, this is

393   the first identification of such complex molecules (diketopiperazines from tripeptide and

394   imidazolidinone from bicyclic amidine) in the pyrolysate of a natural sample.

395   By comparison, pyrochromatograms of the fossil feathers and their 'host' sediment are simpler. They are

396   dominated by *n*-alkane/*n*-alkene doublets (Figs. 8B–C), resulting from the homolytic cleavage of long

397   alkyl chains. In the fossil feathers, these doublets comprise from 8 to 30 carbon atoms, and exhibit a

398   smooth distribution except an intense C_{18} doublet. An additional series of fatty acid methyl esters with

399   alkyl chain ranging from C_8 to C_{30} and maximizing at C_{16} is also identified (Table 2). It results from the

400   release upon pyrolysis of a series of fatty acids that are methylated thanks to TMAH. In addition to these

401   series, a methoxybenzene substituted by two methyl groups or an ethyl group **22** is detected in minor

402   amounts, at the beginning of the pyrochromatogram. A trimethylbenzene and a methylated derivative of

403   methoxyaniline **23** also contribute to this part of the pyrochromatogram. However, the most prominent

404   pyrolysis product **24** corresponds to the C_{18} alcohol methylated through TMAH pyrolysis.

405   The pyrochromatogram of the "host" sediment shares several similarities with that of the fossil feathers.

406   Indeed, it is dominated by series of alkane/alkene doublets and fatty acid methyl esters. Although the

407   distribution of the fatty acid methyl esters is similar in both samples, that of the doublets differs. Indeed,

408   whereas their range ($C_8 - C_{30}$) is similar, the maximum of the series appears at C_{15} in the sediment,

409   instead of a marked predominance of the C_{18} in the fossil (Table 2). Moreover, when comparing the

410   minor compounds eluting at the beginning of the pyrochromatogram, compounds **22** and **23** are common

411   in both samples, whereas a higher number of alkylbenzene homologues occurs in the sediment. Finally,

412   the contribution of octadecanol **24** is much lower in the sediment pyrolysate.

413

414   **DISCUSSION**

415   *Ultrastructure*

416   Microbodies and elongate moulds are observed in feather samples collected at three different locations

417   on *Anchiornis* tail. The elongate shape, parallel orientation and location of the microbodies within the

418   feathers strongly suggest that they correspond to eumelanosomes. These pigment organelles are

419   associated to brown, grey and black hues in modern bird feathers. The preservation of melanosomes, and

420   especially eumelanosomes, in dinosaur feathers is not uncommon. Such microscopic melanin-bearing

421   structures have been described in other theropod dinosaurs, basal birds and isolated feathers (Li *et al*.

422   2010, 2012; Zhang *et al*. 2010; Carney *et al*. 2012; Colleary *et al*. 2015; Pan *et al*. 2016; Hu *et al*. 2018).

423   The chemical composition of these microbodies has been assessed in a previous study, confirming a

424   melanosome origin (Lindgren *et al.* 2015).

425   Recent taphonomic experiments in abiotic conditions suggest that the preservation of mouldic

426   melanosomes requires interaction with an oxidant prior to maturation, and that the preservation of

427   melanosomes is probably less frequent than the preservation of keratinous structures in fossil feathers

428   (Slater *et al*. 2020). It is interesting to see that *Anchiornis* feathers contain both melanosomes and

429   moulds, given their – anoxic – depositional setting. The abiotic nature of the former experiments does

430   however not reflect the depositional and fossilization conditions of *Anchiornis*.

431

432   *Depth profiling, light and heavy element composition*

433   The carbon and nitrogen concentrations determined by EBS led to N/C ratios of 0.33 to 0.42 in modern

434   buzzard feathers, and of 0.08 for the fossil, suggesting a marked relative decrease in nitrogen. The

435   carbon concentration gradient observed by EBS in the fossil feathers of *A. huxleyi* strongly suggests that

436   they are preserved as carbonaceous layers located at the uppermost part of the sample (i.e. $0 - 3$ μm

437   depth, given a rock density of 2.65 g/cm³) and suggests that fossil organic matter could have

438   impregnated the sediment only in a nearby area.

439   The PIXE spectra show elevated concentrations of sulphur in the fossil feathers and, to a lesser extent, in

440   the 'host' sediment, together with very low concentrations in the 'remote' sediment. This suggests that S

441   is associated with the soft tissues. The fossil feathers are therefore preserved as a S-rich carbonaceous

442   film. Substantial quantities of sulphur are present in the modern buzzard feathers ($43,070 \pm 4,236$ ppm

443   in the brown barbs and $37,142 \pm 3,652$ ppm in the rachis, Table 1). This is not surprising due to the

444   presence of sulphur-containing biomacromolecules, such as the pigment phaeomelanin and cysteine- or

445   methionine-containing proteins (i.e. keratins) in bird feathers (Bortolotti 2010; Cesarini 1996; Harrap

446 and Woods 1964; Murphy *et al*. 1990; Riley 1997; Saravanan and Dhurai 2012b). Important studies on

447 the chemical composition of feathers have shown that S is a major element of bird feathers (Harrap and

448 Wood, 1964, 1967; King and Murphy 1987; Murphy *et al*. 1990; Edwards *et al*. 2016). Some authors

449 could even discriminate between organic S originating from keratin and phaeomelanin based on its

450 speciation (Edwards *et al*. 2016). Previous *in situ* chemical analysis (TOF-SIMS) of the melanosomes

451 from the present fossil revealed their enrichment in sulphur with respect to the surrounding sediment,

452 but it could not determine whether it reflects the occurrence of phaeomelanin or diagenetic incorporation

453 of sulphur in eumelanin (Lindgren *et al*. 2015). In a Cretaceous early bird, divalent elements (Cu, Ca,

454 Zn) were suggested to form chelates with melanin (Wogelius *et al*. 2011). Such a complexation may

455 have played a role in sulphur preservation in fossil soft tissues. Alternatively, the presence of sulphur in

456 the fossil feathers can be attributed to natural sulphurization of the organic matter, i.e. the abiogenic

457 intra-molecular incorporation of sulphur from the depositional environment during early diagenesis. The

458 incorporation of sulphur into organic matter was interpreted as a way to enhance the preservation

459 potential of certain labile substances through cross-linking (Sinninghe-Damsté and De Leeuw 1990;

460 Sinninghe-Damsté *et al*. 1989; Sinninghe-Damsté *et al*. 1988; McNamara *et al*. 2016). Indeed, organic

461 matter has the ability to form complexes with inorganic elements, including sulphur, which was traced

462 in fossil soft tissues (e.g. Wogelius *et al*. 2011).

463 *Functional groups in the organic matter*

464 On the whole, the ^{13}C NMR and IR spectra of buzzard feathers (Fig. 6A and 7A) are comparable to that

465 of several keratinous materials, such as feather keratin (Barone *et al*. 2005; Kricheldorf and Müller

466 1984; Wang and Cao 2012, Sharma et al. 2018), wool keratin (Yoshimizu and Ando 1990;

467   Wojciechowska *et al*. 2004) or gecko setae keratin (Jain *et al*. 2015). Indeed, the peak at 173 ppm should

468   mainly correspond to the signal of secondary amide (O=C-NH) groups involved in the peptidic bonds.

469   This is confirmed by the presence of characteristic bands of secondary amides in the IR spectrum of the

470   brown feathers (Fig. 7A). This includes a broad band around 3277 cm^{-1} attributed to the N-H stretching

471   band of amides, a narrow band at 1628 cm^{-1} related to the C=O stretch of Amide I, a band at 1518 cm^{-1}

472   attributed to Amide II and a band at 1237 cm^{-1} related to Amide III (e.g. Bendit 1966; Yu *et al*. 2004;

473   Wang and Cao 2012; Giraldo *et al*. 2013; Tesfaye *et al*. 2017).

474   Carbon atoms bearing both COOH and NH_2 groups (termed C_α) in the amino acids (except glycine)

475   resonate between 50 and 60 ppm in ^{13}C NMR. They account for the peaks at 52.9 and 60.2 ppm in the

476   broad aliphatic signal, whereas the signal at 42.6 ppm is assigned to the C_α of glycine. The other peaks

477   are mainly associated with the amino acid side chains, that at 30.8 ppm being assigned to C_β along with

478   C in long alkyl chains, and those at 19.8 and 25.7 ppm to C_γ and C_δ. The three bands located in the

479   2961-2850 cm^{-1} range in the IR spectra confirms the presence of aliphatic moieties in the modern

480   feathers, although their precise assignment to dedicated compounds is uncertain. In the ^{13}C NMR

481   spectrum, the 129 ppm peak is typical for aromatic carbons, including those from phenylalanine and

482   tyrosine (Jain *et al*. 2015; Yoshimizu and Ando 1990). Finally, the peak at 158 ppm can be ascribed to

483   the O-alkyl C of tyrosine and/or the C of the guanidino group (N-C=N) of arginine (Jain *et al*. 2015;

484   Yoshimizu and Ando 1990). This spectrum is in agreement with previous reports indicating that keratin

485   is a major constituent of feathers (Lucas and Stettenheim 1972). The ^{13}C NMR and IR spectra of the

486   modern feathers also shares some similarities with various types of melanins (Adhyaru *et al*. 2003; Duff

487   *et al*. 1988; Centeno and Shamir 2008; Ito and Nicol 1974).

488   The much simpler ^{13}C NMR spectra of the fossil feathers and their surrounding sediment are dominated

489   by long alkyl chains with a low contribution of aromatic carbons. This is also consistent with the IR

490   spectra (Fig. 7B), mainly showing contributions of aliphatics and silicate and carbonate minerals. When

491   compared to the ^{13}C spectrum of the modern feathers, the aliphatic signal in the fossil is poorly resolved;

492   the aromatic peak is broad and no resonance signal could be detected in the carboxylic region. These

493   features suggest that the proteinaceous contribution identified in the buzzard feathers is no longer

494   present in the fossil sample. The comparison between the FTIR spectrum of the modern feather and that

495   of the fossil feathers (Fig.7A)shows that the characteristic bands of amides are absent in the IR spectrum

496   of the fossil feathers. However, a more precise comparison can be achieved at the molecular level thanks

497   to pyrolysis in the presence of TMAH coupled with GC-MS.

498   *Molecular building blocks of organic matter*

499   TMAH Py-GC-MS analysis of modern feathers thus highlights the presence of glycine, serine, leucine,

500   alanine, valine and proline moieties in buzzard feather keratin, in agreement with previous studies on

501   feather keratin (Fig. 8A; Arai *et al*. 1983, 1986; Murphy *et al*. 1990; O'Donnell and Inglis 1974;

502   Saravanan and Dhurai 2012b; Staroń *et al*. 2011). Additionally, pyrolysis products derived from

503   isoleucine, phenylalanine and tyrosine occurred in substantial amounts although they are often

504   considered as minor constituents of feather keratin. However, homolysis of the side chain of

505   phenylalanine and tyrosine favours high yields in TMAH pyrolysis (Gallois *et al*. 2007). Despite its

506   acknowledged high abundance in feather keratin, cysteine is absent in the pyrochromatogram of buzzard

507   feathers, probably because it mainly releases H_2S upon pyrolysis (Moldoveanu 2009) not detected in the

508   presently used analytical conditions. Alternatively, some of the identified products (methylbenzene **1**,

509   methyl, methoxybenzene **9**) as well as glycine derivatives may originate from melanin, although they are

510   poorly diagnostic compounds (Stępień *et al*. 2009). However, the melanin signal was reported to be

511   overwhelmed by protein-derived products upon pyrolysis of bulk feathers (Barden *et al*. 2011).

512   The pyrochromatograms of the fossil feathers and their 'host' sediment are comparable as they are both

513   dominated by series of alkane/alkene doublets and fatty acid methyl esters as well as minor compounds

514   eluting at the beginning of the pyrochromatogram. The latter include a methoxybenzene substituted by

515   two methyl groups or an ethyl group **22** which originates from lignin or polysaccharides such as

516   cellulose, depending on its substitution pattern (Choi *et al*. 2013; Seitz and Ram 2000). Despite these

517   similarities, differences are observed, including the much weaker abundance of octadecanol **24** in the

518   sediment pyrolysate. These differences clearly show that even though some imprint from the sediment

519   may have contributed to the fossil feather pyrolysate, at least some features are typical for the fossil

520   feathers. They notably include the C_{18} doublet and octadecanol **24**. The predominance of the

521   alkane/alkene doublets in the pyrolysate is in agreement with the strong aliphatic signal observed in

522   NMR and FTIR (bands at 2690, 2920 and 2851 cm^{-1}) (Figs. 6–7). A similar highly aliphatic character

523   has been reported in Eocene bird feathers (O'Reilly *et al*. 2017) but also in soft tissues from other fossil

524   organisms, such as in cuticles from Carboniferous arthropods (Baas *et al*. 1995; Stankiewicz *et al*.

525   1998), skin from a Cretaceous mummified hadrosaur (Manning *et al*. 2009), and Cretaceous fish scales

526   (Gupta *et al*. 2008). C_1 to C_3 alkylbenzenes were also identified in pyrolysates of Oligocene weevil and

527   tadpole, and associated matrix (Barden *et al*. 2015; Gupta *et al*. 2007).

528   The aliphatic series dominating the pyrolysate of the fossil feathers reflect either selective preservation

529   of macromolecular aliphatic matter pre-existing in the extant organism (Tegelaar *et al*. 1989) or *in situ*

25

530   polymerization of aliphatic lipids (Gupta *et al.* 2007; Stankiewicz *et al.* 2000). No such aliphatic series

531   could be detected in the pyrolysate of modern feathers, likely precluding the first hypothesis. In contrast,

532   several aliphatic series were identified in the lipid extract of the modern feathers (*n*-alkanes, *n*-acids, *n*-

533   alcohols; data not shown). Indeed, modern bird feathers are coated by lipids as protection against

534   adverse environmental factors. Such lipids, secreted by the uropygial gland, were recently shown to be

535   preserved through geopolymerisation in an Eocene bird (O'Reilly *et al.* 2017). A similar

536   geopolymerisation can be put forward to account for the occurrence of aliphatic moieties of the present

537   fossil feathers. Endogenous lipids may be transformed into more stable geopolymers, composed of

538   alkane/alkene doublets, and can therefore be 'preserved' and traced in vertebrate fossils (O'Reilly *et al.*

539   2018).

540   The absence of signals typical for proteinaceous material in the NMR and IR spectra and

541   pyrochromatogram of the fossil feathers is noteworthy. It is further suggested by the weak N/C ratio in

542   the fossil when compared with modern feathers. The lack of proteinaceous components consistent with

543   keratin was previously suggested on the same fossil based on TOF-SIMS and IR analyses (Lindgren *et*

544   *al.*, 2015). In agreement with the commonly accepted lability of proteins, this feature suggests their

545   extensive degradation in our specimen upon diagenesis. Recent taphonomy experiments on extant

546   feathers demonstrated substantial degradation of keratin upon microbial and thermal decay (Saitta *et al.*

547   2017). Moreover, it must be noted that diagenetic degradation of proteinaceous moieties was previously

548   put forward for Eocene birds (Saitta *et al.* 2017; O'Reilly *et al.* 2017) and Palaeozoic annelid fossils

549   (Dutta *et al.* 2010). However, even if no proteinaceous compounds were detected in *Anchiornis* feathers,

550   one cannot exclude the possibility of finding similar biomolecules preserved in other fossils in the

551   future.

552   Although PIXE analyses showed that carbon and sulphur are closely associated in the fossil feathers, no

553   organosulphur compound could be detected in the pyrolysate. Altogether, the lack of organosulphur

554   compounds (such as thiophenes) in the fossil feather pyrolysates and the lack of C=S/C-S species in

555   their IR spectrum strongly suggest a lack of organic-S species in this sample. In contrast, sulphur

556   incorporation was evidenced through FTIR and TMAH-Py-GC-MS in melanosomes of Miocene frogs,

557   thus demonstrating involvement of natural sulphurization in the preservation of the fossil organic matter

558   (McNamara *et al*., 2016). The lack of organosulphur compounds in *Anchiornis* pyrolysate should thus

559   reflect diagenetic conditions that prevented such natural sulphurization of organic matter. In the

560   sedimentary environment, the sulphurization of organic matter to form organosulphur compounds

561   requires the presence of reactive organic matter and inorganic sulphides (i.e. anoxic conditions), with

562   sufficient, but not excessive, reactive iron. If reactive iron exceeds a certain quantity, iron sulphides

563   (pyrite) would precipitate instead (Werne *et al*. 2000; Canfield 1989). Here, our results suggest that the

564   concentration of sulphur and iron in the environment was high enough to form iron sulphides (i.e. pyrite

565   framboids and microcrystallites). The occurrence of iron oxides or hydroxides as framboid crystals

566   (SEM and EDX characterization) suggests that sulphur may have been preferentially used for the

567   formation of iron sulphides (such as pyrite) during early diagenesis (Sinninghe-Damsté and De Leeuw

568   1990). During later diagenesis, pyrite framboids were probably *in situ* weathered into the iron oxides and

569   hydroxides observed beneath the carbonaceous surface of feathers, thus releasing sulphur that may have

570   been further associated with organic compounds, e.g. through the formation of chelate with melanin

571   (Wogelius *et al*. 2011). Such associations may have favoured/enhanced organic matter preservation and

572   are consistent with the interrelation between sulphur and carbon highlighted by PIXE analyses.

573   Recently, a mechanism of nitrogen preservation based on lipoxidation and glycoxidation of protein was

574   proposed in biomineralized tissues of diverse Mesozoic and Cenozoic vertebrates, fossilized in oxidative

575   settings (Wiemann *et al*. 2018). Such a process, which can be catalysed by transition metal such as iron,

576   may have led to the preservation of the small amount of nitrogen in YFGP-T5199. However, the present

577   study deals with soft tissues and not biomineralized one. Additionally, so far this preservation

578   mechanism could only be evidenced in oxidizing environment (Wiemann *et al*. 2018). The occurrence of

579   iron oxide framboids in the studied *Anchiornis* fossil probably resulting from pyrite weathering, rather

580   attests for the reducing conditions of fossilisation, thus making unlikely the involvement of this

581   preservation pathway (i.e. lipoxidation).

582   Further experimental studies on modern feathers and comparisons with the fossil record are required to

583   explain why keratin is not preserved in *Anchiornis* feathers although melanin has been detected, and

584   melanosomes and moulds have been observed.

585

586   **CONCLUSIONS**

587

588   The methods used in this study provide new and complementary information on how the plumage of

589   *Anchiornis huxleyi* (YFGP-T5199) is preserved. SEM and EDS reveal that fossil feathers are preserved

590   in a fine-grained material constituted of K-rich phyllosilicates, illite and interstratified illite/smectite.

591   PIXE analyses show that both light (C, N, O) and heavy (S, Na, Ca, etc.) elements are present in the

592   fossil samples, even at very low concentrations. The presence of iron oxide pseudomorphs after pyrite

593   likely indicates a reduced depositional environment for *Anchiornis*. Carbon is the dominant element in

594 the fossil feathers, which are also enriched in sulphur with respect to the 'host' sediment. EBS mapping

595 of the interior of the samples revealed a decrease in carbon concentration with depth. Our analysis

596 therefore shows that the fossil feathers are preserved in the uppermost part of the sample, as a thin – ca.

597 3 μm-thick – S-bearing carbonaceous layer. High resolution imaging of the feather microstructure

598 revealed the presence of elongated microbodies (650-950 nm), likely corresponding to eumelanosomes.

599 Molecular characterization of the organic matter in the 'host' sediment, fossil feathers and modern

600 feathers by ^{13}C-NMR, micro-ATR FTIR and Py-GC-MS shows that the fossil does not display the

601 complex amino-acid signature typical for keratin, the main constituent of modern feathers. Although the

602 organic matter of the fossil feathers and their 'host' sediment are both dominated by aliphatic moieties,

603 they exhibit substantial differences (distribution pattern of series, occurrence of components specific to

604 the feathers) suggesting that the organic matter of the fossil feathers is derived, at least partially, from

605 original constituents of the feathers.

606 Altogether, these results show that the fossil feathers can be described as compression fossils, as

607 described in Schweitzer (2011: p. 192). The finely grained (clay-rich) host sediment contributed to the

608 morphological preservation of *Anchiornis* soft tissues. As stressed by Schweitzer (2011: p. 192), the

609 very fine grain size of the sediments might have prevented the degradation of soft tissues by microbes,

610 and subsequent loss of degraded organic matter in the environment before and during diagenesis.

611 However, the lack of protein-derived moieties in the fossil organic matter shows that the latter has been

612 significantly altered during diagenesis. The excellent morphological preservation of the fossil soft tissue

613 is not associated here with a high preservation level of organic matter. Hence, the fossil feathers have

614 likely undergone a complex diagenetic history including several steps affecting differentially their

615 morphology and chemistry. *In situ* polymerization of lipids into more stable aliphatic compounds during

616 early diagenesis was likely the main process responsible for organic matter preservation in the fossil

617 feathers. Additionally, sulphur was probably involved in several steps of the fossil preservation although

618 no natural sulphurization took place.

619 Our results are therefore unique by combining different analytical techniques on Jurassic fossil feathers.

620 This integrative multidisciplinary study appears as a powerful approach to decipher morphological,

621 mineralogical, structural and chemical features of fossil soft tissues and their fossilization processes.

622 This study provides new insights into the taphonomy of labile compounds, suggesting that keratin,

623 unlike the pigment melanin, is not present in the feathers of YFGP- T5199.Our results question the

624 preservation potential of keratin (and melanin) in anoxic conditions. Further analyses of fossil feathers

625 of different ages and deposited in different environmental settings, are required to better understand the

626 preservation potential of melanin and keratin.

627

628 Finally, we used here for the first time on a Jurassic fossil Ion Beam Analysis (IBA), a non-destructive

629 analytical technique providing an in-depth profiling of C to U elements. Further developments of this

630 technique to palaeontological samples might help at identifying the precise location of fossil soft tissues

631 within the sediment and then characterizing metal elements that are directly associated with the

632 fossilised tissues.

641

DATA ARCHIVING STATEMENT

643   Additional data for this study are available in the [Dryad Digital Repository]:

644   https://datadryad.org/review?doi=doi:10.5061/dryad.XXXX

645

646

REFERENCES

648

649   ADHYARU, B. B., AKHMEDOV, N. D., KATRITZKY, A. R. and BOWERS, C. R. 2003. Solid-state

650   cross-polarization magic angle spinning ^{13}C and ^{15}N NMR characterization of Sepia melanin,

651   Sepia melanin free acid and Human hair melanin in comparison with several model compounds.

652   *Magnetic resonance in chemistry*, **41**, 466-474.

653   ALLISON, P. A. and BRIGGS, D. E. G. 1993. Exceptional fossil record: Distribution of soft-tissue

654   preservation through the Phanerozoic. *Geology*, **21**, 527-532.

655   ARAI, K. M., TAKAHASHI, R., YOKOTE, Y. and AKAHANE, K. 1983. Amino acid sequence of

656   feather keratin from fowl. *The FEBS Journal*, **132** (3), 501-507.

657 —— 1986. The primary structure of feather keratins from duck (*Anas platyrhynchos*) and pigeon

658   (*Columba livia*). *Biochimica et Biophysica Acta (BBA)-Protein Structure and Molecular*

659   *Enzymology*, **873** (1), 6-12.

660 BAAS, M., BRIGGS, D., VAN HEEMST, J., KEAR, A. and DE LEEUW, J. 1995. Selective

661   preservation of chitin during the decay of shrimp. *Geochimica et Cosmochimica Acta*, **59** (5),

662   945-951.

663 BARDEN, H. E., WOGELIUS, R. A., LI, D., MANNING, P. L., EDWARDS, N. P. and VAN

664   DONGEN, B. E. 2011. Morphological and geochemical evidence of eumelanin preservation in

665   the feathers of the Early Cretaceous bird, *Gansus yumenensis*. *PLoS One*, **6** (10), e25494

666 BARDEN, H. E., BERGMANN, U., EDWARDS, N. P., EGERTON, V. M., MANNING, P. L.,

667   PERRY, S., VAN VEELEN, A., WOGELIUS, R. A. and VAN DONGEN, B.E. 2015. Bacteria

668   or melanosomes? A geochemical analysis of micro-bodies on a tadpole from the Oligocene

669   Enspel Formation of Germany. *Palaeobiodiversity and Palaeoenvironments*, **95** (1), 33-45.

670 BARONE, J. R., SCHMIDT, W. F. and LIEBNER, C. F. E. 2005. Thermally processed keratin films.

671   *Journal of Applied Polymer Science*, **97**, 1644-1651.

672 BARTHEL, K. 1964. Zur Entstehung der Solnhofer Plattenkalke (unteres Untertithon). *Mitteilungen der*

673   *Bayerischen Staatssammlung für Paläontologie und Historische Geologie*, **4**, 37-69.

674 BASIUK, V. A. and NAVARRO-GONZÁLEZ, R. 1997. Identification of hexahydroimidazo [1, 2-a]

675   pyrazine-3, 6-diones and hexahydroimidazo [1, 2-a] imidazo [1, 2-d] pyrazine-3, 8-diones,

676   unusual products of silica-catalyzed amino acid thermal condensation and products of their

677   thermal decomposition using coupled high-performance liquid chromatography–particle beam

678   mass spectrometry and gas chromatography–Fourier transform infrared spectroscopy–mass

679   spectrometry. *Journal of Chromatography A*, **776** (2), 255-273.

680   BECK, L. 2014. Recent trends in IBA for cultural heritage studies. *Nuclear Instruments and Methods in*

681   *Physics Research B*, **332**, 439-444.

682   BENDIT, E.G. 1966. Infrared absorption spectrum of keratin. I. Spectra of α-, β-, and supercontracted

683   keratin. *Biopolymers*, **4**, 539-559.

684   BENTON, M. J., ZHONGHE, Z., ORR, P. J., FUCHENG, Z. and KEARNS, S. L. 2008. The remarkable

685   fossils from the Early Cretaceous Jehol Biota of China and how they have changed our

686   knowledge of Mesozoic life. *Proceedings of the Geologists' Association*, **119**, 209-229.

687   BLANCO, A., BOLAÑOS-SÁNCHEZ, U., LIZÁRRAGA-MENDIOLA, L., HERNÁNDEZ-ÁVILA, J.,

688   ÁNGELES-TRIGUEROS, S., AMBROCIO, P. and GONZÁLEZ-SANDOVAL, M. 2013.

689   Microscopic evidences of replacement of iron sulfide by iron oxide in macro fossils: a useful tool

690   for the search of life in Mars? *Lunar and Planetary Science Conference*, **44**, 2956.

691   BORTOLOTTI, G. R. 2010. Flaws and pitfalls in the chemical analysis of feathers: bad news–good

692   news for avian chemoecology and toxicology. *Ecological Applications*, **20** (6), 1766-1774.

693   BRIGGS, D. E. G., KEAR, A., MARTILL, D. and WILBY, P. 1993. Phosphatization of soft-tissue in

694   experiments and fossils. *Journal of the Geological Society*, **150** (6), 1035-1038.

695   BRIGGS, D. E. G., BOTTRELL, S. H. and RAISWELL, R. 1991. Pyritization of soft-bodied fossils:

696   Beecher's trilobite bed, Upper Ordovician, New York State. *Geology*, **19** (12), 1221-1224.

697   BUTTERFIELD, N. J., BALTHASAR, U. and WILSON, L. A. 2007. Fossil diagenesis in the Burgess

698   Shale. *Palaeontology*, **50** (3), 537-543.

699   CAMPBELL, J., BOYD, N., GRASSI, N., BONNICK, P. and MAXWELL, J. 2010. The Guelph PIXE

700   software package IV. *Nuclear Instruments and Methods in Physics Research Section B: Beam*

701   *Interactions with Materials and Atoms*, **268** (20), 3356-3363.

702   CANFIELD, D. E. 1989. Reactive iron in marine sediments. *Geochemica and Cosmochemica Acta*, **53**

703   (**3**), 619-632.

704   CENTENO, S. A. and SHAMIR, J. 2008. Surface enhanced Raman scattering (SERS) and FTIR

705   characterization of the sepia melanin pigment used in works of art. *Journal of Molecular*

706   *Structure*, **873** (1-3), 149-159.

707   CESARINI, J. P. 1996. Melanins and their possible roles through biological evolution. *Advances in*

708   *space research,* **18** (12), 35-40.

709   CHANG, S. C., ZHANG, H., RENNE, P. R. and FANG, Y. 2009. High-precision ^{40}Ar/^{39}Ar age

710   constraints on the basal Lanqi Formation and its implications for the origin of angiosperm plants.

711   *Earth and Planetary Science Letters*, **279** (3), 212-221.

712   CHOI, S. S., KIM, M. C. and KIM, Y. K. 2013. Formation of methoxybenzenes from cellulose in the

713   presence of tetramethylammonium hydroxide by pyrolysis. *Bulletin of the Korean Chemical*

714   *Society*, **34** (2), 649-652.

715   CHRISTIANSEN, P. and BONDE, N. 2004. Body plumage in *Archaeopteryx*: a review and new

716   evidence from the Berlin specimen. *Comptes Rendus Palevol*, **3** (2), 99-118.

717   CHU, Z., HE, H., RAMEZANI, J., BOWRING, S. A., HU, D., ZHANG, L., ZHENG, S., WANG, X.,

718   ZHOU, Z. and DENG, C. 2016. High-precision U-Pb geochronology of the Jurassic Yanliao

719   Biota from Jianchang (western Liaoning Province, China): Age constraints on the rise of

720   feathered dinosaurs and eutherian mammals. *Geochemistry, Geophysics, Geosystems*, **17** (10),

721   3983-3992.

722 CINCOTTA, A., PESTCHEVITSKAYA, E. B., SINITSA, S. M., MARKEVICH, V. S., DEBAILLE,

723   V., RESHETOVA, S. A., MASHCHUK, I. M., FROLOV, A. O., GERDES, A., YANS, J. and

724   GODEFROIT, P. 2019. The rise of feathered dinosaurs: Kulindadromeus zabaikalicus, the oldest

725   dinosaur with 'feather-like'structures. *PeerJ*, **7**, e6239.

726 COLLEARY, C., DOLOCAN, A., GARDNER, J., SINGH, S., WUTTKE, M., RABENSTEIN, R.,

727   HABERSETZER, J., SCHAAL, S., FESEHA, M. and CLEMENS, M. 2015. Chemical,

728   experimental, and morphological evidence for diagenetically altered melanin in exceptionally

729   preserved fossils. *Proceedings of the National Academy of Sciences*, **112** (41), 12592-12597.

730 DAVIS, J. A. 1984. Complexation of trace metals by adsorbed natural organic matter. *Geochimica et*

731   *Cosmochimica Acta*, **48** (4), 679-691.

732 DUFF, G. A., ROBERTS, J. E. and FOSTER, N. 1988. Analysis of the structure of synthetic and natural

733   melanins by solid-phase NMR. *Biochemistry*, **27**, 7112-7116.

734 DUTTA, S., HARTKOPF-FRÖDER, C., MANN, U., WILKES, H., BROCKE, R. and BERTRAM, N.

735   2010. Macromolecular composition of Palaeozoic scolecodonts: insights into the molecular

736   taphonomy of zoomorphs. *Lethaia*, **43** (3), 334-343.

737 FARRELL, Ú. C., BRIGGS, D. E. G., HAMMARLUND, E. U., SPERLING, E. A. and GAINES, R. R.

738   2013. Paleoredox and pyritization of soft-bodied fossils in the Ordovician Frankfort Shale of

739   New York. *American Journal of Science*, **313** (5), 452-489.

740 FRASER, R. D. B. and MACRAE, T. P. 2012. *Conformation in fibrous proteins and related synthetic*

741   *polypeptides*. Academic press, London, 648 pp.

742   FRASER, R. D. B. and PARRY, D. A. D. 1996. The molecular structure of reptilian keratin.

743   *International Journal of Biological Macromolecules*, **19** (3), 207-211.

744   GABBOTT, S., NORRY, M., ALDRIDGE, R. and THERON, J. 2001. Preservation of fossils in clay

745   minerals; a unique example from the Upper Ordovician Soom Shale, South Africa. *Proceedings*

746   *of the Yorkshire Geological Society*, **53** (3), 237-244.

747   GALLOIS, N., TEMPLIER, J. and DERENNE, S. 2007. Pyrolysis-gas chromatography-mass

748   spectrometry of the 20 protein amino acids in the presence of TMAH. *Journal of Analytical and*

749   *Applied Pyrolysis*, **80**, 216-230.

750   GODEFROIT, P., CAU, A., DONG-YU, H., ESCUILLIÉ, F., WENHAO, W. and DYKE, G. 2013. A

751   Jurassic avialan dinosaur from China resolves the early phylogenetic history of birds. *Nature*,

752   **498 (7**454), 359-362.

753   GODEFROIT, P., SINITSA, S. M., DHOUAILLY, D., BOLOTSKY, Y. L., SIZOV, A. V.,

754   MCNAMARA, M. E., BENTON, M. J. and SPAGNA, P. 2014. A Jurassic ornithischian

755   dinosaur from Siberia with both feathers and scales. *Science*, **345** (6).

756   GODEFROIT, P., SINITSA, S. M., CINCOTTA, A., MCNAMARA M. E., RESHETOVA, S. A. and

757   DHOUAILLY, D. 2020. Integumentary structures in *Kulindadromeus zabaikalicus*, a Basal

758   Neornithischian Dinosaur from the Jurassic of Siberia. In FOTH, C. and RAUHUT, O. W. M.

759   (eds.). *The Evolution of Feathers*. Springer, Switzerland, 47-65.

760   GRADSTEIN, F. M., OGG, J. G., SCHMITZ, M. and OGG, G. 2012. The geologic time scale 2012.

761   Elsevier.

762 GREGG, K. and ROGERS, G. E.. 1986. Feather keratin: composition, structure and biogenesis. *In*

763 BEREITER-HAHN, J., MATOLSKY, A. G. and RICHARDS, K. S. (eds). *Biology of the*

764 *integument*. Springer, Berlin, Heidelberg, 666-694.

765 GUPTA, N. S., CAMBRA-MOO, O., BRIGGS, D. E., LOVE, G. D., FREGENAL-MARTINEZ, M. A.

766 and SUMMONS, R. E. 2008. Molecular taphonomy of macrofossils from the Cretaceous Las

767 Hoyas Formation, Spain. *Cretaceous Research*, **29** (1), 1-8.

768 GUPTA, N. S., MICHELS, R., BRIGGS, D. E., COLLINSON, M. E., EVERSHED, R. P. and

769 PANCOST, R. D. 2007. Experimental evidence for the formation of geomacromolecules from

770 plant leaf lipids. Organic *Geochemistry*, **38** (1), 28-36.

771 GURBICH, A. 2016. SigmaCalc recent development and present status of the evaluated cross-sections

772 for IBA. *Nuclear Instruments and Methods in Physics Research Section B: Beam Interactions*

773 *with Materials and Atoms*, **371**, 27-32.

774 HARMS, F. 2002. Steine erzählen Geschichte (n): Ursache für die Entstehung des Messel-Sees

775 gefunden. *Natur und Museum*, **132** (1), 1-4.

776 HARRAP, B. S. and WOODS, E. F. 1964. Soluble derivatives of feather keratin: 1. Isolation,

777 fractionation and amino acid composition. *Biochemical journal*, **92** (1), 8.

778 — 1967. Species differences in the proteins of feathers. *Comparative Biochemistry and Physiology*, **20**

779 (2), 449-460

780 HENDRICKER, A. D. and VOORHEES, K. J. 1996. An investigation into the Curie-point pyrolysis-

781 mass spectrometry of glycyl dipeptides. *Journal of Analytical and Applied Pyrolysis*, **36** (1), 51-

782 70.

783   HEIMHOFER, R. and MARTILL, D. 2007. The sedimentology and depositional environment of the

784   Crato Formation. *In* MARTILL, D. M., BECHLY, G. and LOVERIDGE, R. F. (eds). *The Crato*

785   *fossil beds of Brazil: a window into an ancient world*. Cambridge University Press, 44-62.

786   HU, D., HOUL, L., ZHANG, L. and XU, X. 2009. A pre-*Archaeopteryx* troodontid theropod from

787   China with long feathers on the metatarsus. *Nature*, **461** (7264), 640.

788   ITO, S. and NICOL, J. C. 1974. Isolation of oligomers of 5, 6-dihydroxyindole-2-carboxylic acid from

789   the eye of the catfish. *Biochemical Journal*, **143** (1), 207-217.

790   JAIN, D., STARK, A. Y., NIEWIAROWSKI, P. H., MIYOSHI, T. and DHINOJWALA, A. 2015. NMR

791   spectroscopy reveals the presence and association of lipids and keratin in adhesive gecko setae.

792   *Scientific Reports*, **5** (9594).

793   JEYNES, C., BARRADAS, N., MARRIOTT, P., BOUDREAULT, G., JENKIN, M., WENDLER, E.

794   and WEBB, R. 2003. Elemental thin film depth profiles by ion beam analysis using simulated

795   annealing-a new tool. *Journal of Physics D: Applied Physics*, **36** (**7**0), R97.

796   JEYNES, C. and COLAUX, J. L. 2016. Thin film depth profiling by ion beam analysis. *Analyst*, **141**

797   (21), 5944-5985.

798   JI, Q. and JI, S. 1996. On the Discovery of the earliest fossil bird in China (*Sinosauropteryx* gen. nov.)

799   and the origin of birds. *Chinese Geology*, **233**, 6.

800   KAYE, T. G., GAUGLER, G. and SAWLOWICZ, Z. 2008. Dinosaurian soft tissues interpreted as

801   bacterial biofilms. *PLoS ONE*, **3** (7), e2808.

802   KELLNER, A. W., WANG, X., TISCHLINGER, H., DE ALMEIDA CAMPOS, D., HONE, D. W. and

803   MENG, X. 2010. The soft tissue of Jeholopterus (Pterosauria, Anurognathidae,

804   Batrachognathinae) and the structure of the pterosaur wing membrane. *Proceedings of the Royal*

805   *Society of London B: Biological Sciences*, **277** (1679), 321-329.

806 KELLNER, A. W. A. and DE ALMEIDA CAMPOS, D. 2002. The function of the cranial crest and jaws

807   of a unique pterosaur from the Early Cretaceous of Brazil. *Science*, **297**, 389-392.

808 KING, J. R. and MURPHY, M. E. 1987. Amino acid composition of the calamus, rachis, and barbs of

809   white-crowned sparrow feathers. *The Condor*, **89** (2), 436-439.

810 KRICHELDORF, H. R. and MÜLLER, D. 1984. Secondary structure of peptides 16th. Characterization

811   of proteins by means of ^{13}C NMR CP/MAS spectroscopy. *Colloid & Polymer Science*, **262**, 856-

812   861.

813 LENG, Q. and YANG, H. 2003. Pyrite framboids associated with the Mesozoic Jehol biota in

814   northeastern China: implications for microenvironment during early fossilization. *Progress in*

815   *Natural Science*, **13** (3), 206-212.

816 LI, Q., GAO, K. -Q., VINTHER, J., SHAWKEY, M. D., CLARKE, J. A., D'ALBA, L., MENG, Q.,

817   BRIGGS, D. E. G. and PRUM, R. O. 2010. Plumage color patterns of an extinct dinosaur.

818   *Science*, **327**, 1369-1372.

819 LI, Q., GAO, K. -Q., MENG, Q., CLARKE, J. A., SHAWKEY, M. D., D'ALBA, L., PEI, R.,

820   ELLISON, M., NORELL, M. A. and VINTHER, J. 2012. Reconstruction of *Microraptor* and the

821   evolution of iridescent plumage. *Science*, **335**, 1215.

822 LINDGREN, J., SJÖVALL, P., CARNEY, R. M., CINCOTTA, A., UVDAL, P., HUTCHESON, S. W.,

823   GUSTAFSSON, O., LEFÈVRE, U., ESCUILLIER, F., HEIMDAL, J., ENGDAHL, A., GREN,

824   J. A., KEAR, B. P., WAKAMATSU, K., YANS, J. and GODEFROIT, P. 2015. Molecular

825   composition and ultrastructure of Jurassic paravian feathers. *Scientific Reports*, 5(13520).

826 LIU, Y. Q., KUANG, H. W., JIANG, X. J., PENG, N., XU, H. and SUN, H. Y. 2012. Timing of the

827   earliest known feathered dinosaurs and transitional pterosaurs older than the Jehol Biota.

828   *Palaeogeography, Palaeoclimatology, Palaeoecology*, **323-325**, 1-12.

829 LUCAS, A. M., and P. R. STETTENHEIM. 1972. *Avian anatomy: Integuments*. U.S. Department of

830   Agriculture in cooperation with Michigan Agricultural Experiment Station, Washington D.C.

831 MANNING, P. L., P. M. MORRIS, A. MCMAHON, E. JONES, A. GIZE, J. H. MACQUAKER, G.

832   WOLFF, A. THOMPSON, J. MARSHALL, and K. G. TAYLOR. 2009. Mineralized soft-tissue

833   structure and chemistry in a mummified hadrosaur from the Hell Creek Formation, North Dakota

834   (USA). *Proceedings of the Royal Society of London B: Biological Sciences*, **276** (1672), 3429-

835   3437.

836 MANNING, P. L., N. P. EDWARDS, R. A. WOGELIUS, U. BERGMANN, H. E. BARDEN, P. L.

837   LARSON, D. SCHWARZ-WINGS, V. M. EGERTON, D. SOKARAS, and R. A. MORI. 2013.

838   Synchrotron-based chemical imaging reveals plumage patterns in a 150 million year old early

839   bird. *Journal of Analytical Atomic Spectrometry*, **28** (7), 1024-1030.

840 MARTILL, D. M. and HEIMHOFER, U. 2007. Stratigraphy of the Crato Formation. *In* MARTILL, D.

841   M., BECHLY, G. and LOVERIDGE, R. F. *The Crato fossil beds of Brazil: window into an*

842   *ancient world*. Cambridge University Press, 25-43.

843 MARTIN, D., BRIGGS, D. E. and PARKES, R. J. 2004. Experimental attachment of sediment particles

844   to invertebrate eggs and the preservation of soft-bodied fossils. *Journal of the Geological*

845   *Society*, **161** (5), 735-738.

846 MAYR, G., PETERS, D. S., PLODOWSKI, G. and VOGEL, O. 2002. Bristle-like integumentary

847   structures at the tail of the horned dinosaur *Psittacosaurus*. *Naturwissenschaften*, **89**, 361-365.

848 MCNAMARA, M. E., VAN DONGEN, B. E., LOCKYER, N. P., BULL, I. D. and ORR, P. J. 2016.

849 Fossilization of melanosomes via sulfurization. *Palaeontology,* **59** (3), 1-14.

850 MOLDOVEANU, S. C. 2009. Pyrolysis of organic molecules: applications to health and environmental

851 issues. *In* techniques and instrumentation in analytical chemistry, Elsevier, **28**, 723pp.

852 MOYER, A. E., ZHENG, W. and SCHWEITZER, M. H. 2016. Keratin durability has implications for

853 the fossil record: results from a 10 year feather degradation experiment. *PloS One*, **11** (7),

854 e0157699.

855 MURPHY, M. E., KING, J. R., TARUSCIO, T. G. and GEUPEL, G. R. 1990. Amino acid composition

856 of feather barbs and rachises in three species of pygoscelid penguins: nutritional implications.

857 *The Condor*, **92** (4), 913-921.

858 NAN, P., YONGQING, L., HONGWEI, K., XIAOJUN, J. and HUAN, X. 2012. Stratigraphy and

859 geochronology of vertebrate fossil-bearing Jurassic strata from Linglongta, Jianchang County,

860 Western Liaoning, Northeastern China. *Acta Geologica Sinica* (English Edition), **86** (6), 1326-

861 1339.

862 NORDSTROM, D. K. 1982. Aqueous pyrite oxidation and the consequent formation of secondary iron

863 minerals. *In* KITTRICK, J. A., FANNING, D. S. and HOSSNER, L. R. (eds), *Acid Sulfate*

864 *Weathering*. Soil Science Society of America, Spec. Publ. 10, Madison, 37-56.

865 O'DONNELL, I. and INGLIS, A. 1974. Amino acid sequence of a feather keratin from Silver Gull

866 (*Larus novae-hollandiae*) and comparison with one from Emu (*Dromaius novae-hollandiae*).

867 *Australian journal of biological sciences*, **27** (4), 369-382.

868 O'REILLY, S., SUMMONS, R., MAYR, G. and VINTHER, J. 2018. Preservation of uropygial gland

869 lipids in a 48-million-year-old bird. *Proceedings of the Royal Society B*, **284**, 20071050.

870   PAN, Y., SHA, J., ZHOU, Z. and FÜRSICH, F. T. 2013. The Jehol Biota: definition and distribution of

871   exceptionally preserved relics of a continental Early Cretaceous ecosystem. *Cretaceous*

872   *Research*, **44**, 30-38.

873   PAN, Y., ZHENG, W., MOYER, A. E., O'CONNOR, J. K., WANG, M., ZHENG, X., Wang, X.,

874   SCHROETER, E. R., ZHOU, Z. and SCHWEITZER, M. H. 2016. Molecular evidence of keratin

875   and melanosomes in feathers of the Early Cretaceous bird Eoconfuciusornis. *Proceedings of the*

876   *National Academy of Sciences*, **113** (49), E7900-E7907.

877   PAN, Y., ZHENG, W., SAWYER, R. H., PENNINGTON, M. W., ZHENG, X., WANG, X., WANG,

878   M., HU, L., O'CONNOR, J., ZHAO, T. and LI, Z. 2019. The molecular evolution of feathers

879   with direct evidence from fossils. *Proceedings of the National Academy of Sciences*, **116** (8),

880   3018-3023.

881   RAUHUT, O. W., FOTH, C., TISCHLINGER, H. and NORELL, M. A. 2012. Exceptionally preserved

882   juvenile megalosauroid theropod dinosaur with filamentous integument from the Late Jurassic of

883   Germany. *Proceedings of the National Academy of Sciences*, **109** (29), 11746-11751.

884   RILEY, P. A. 1997. Melanin. *The international journal of biochemistry & cell biology*, **29** (11), 1235-

885   1239.

886   SAITTA, E.T., ROGERS, C., BROOKER, R.A., ABBOTT, G.D., KUMAR, S., O'REILLY, S.S.,

887   DONOHOE, P., DUTTA, S., SUMMONS, R.E. and VINTHER, J. 2017. Low fossilization

888   potential of keratin protein revealed by experimental taphonomy. *Palaeontology*, **60** (4), 547-

889   556.

890   SARAVANAN, K. and DHURAI, B. 2012. Exploration on amino acid content and morphological

891   structure in chicken feather fiber. *Journal of Textile and Apparel, Technology and Management*,

892   **7** (3), 1-6.

893   SCHWEITZER, M. H., WATT, J. A., AVCI, R., FORSTER, C. A., KRAUSE, D. W., KNAPP, L.,

894   ROGERS, R. R., BEECH, I. and MARSHALL, M. 1999. Keratin immunoreactivity in the Late

895   Cretaceous bird *Rahonavis ostromi*. *Journal of Vertebrate Paleontology*, **19** (4), 712-722.

896   SCHWEITZER, M. H. 2011. Soft tissue preservation in terrestrial Mesozoic vertebrates. Annual Review

897   of *Earth and Planetary Sciences*, **39**, 187-216.

898   SEITZ, L. M. and RAM, M. 2000. Volatile methoxybenzene compounds in grains with off-odors.

899   *Journal of agricultural and food chemistry*, **48** (9), 4279-4289.

900   SHARMA, S., GUPTA, A., KUMAR, A., KEE, C. G., KAMYAB, H. and SAUFI, S. M. 2018. An

901   efficient conversion of waste feather keratin into ecofriendly bioplastic film. *Clean Technologies*

902   *and Environmental Policy*, **20** (10), 2157-2167.

903   SIMMONDS, P., MEDLEY, E., RATCLIFF, M. and SHULMAN, G. 1972. Thermal decomposition of

904   aliphatic monoaminomonocarboxylic acids. *Analytical chemistry*, **44** (12), 2060-2066.

905   SINNINGHE-DAMSTÉ, J. S. and DE LEEUW, J. W. 1990. Analysis, structure and geochemical

906   significance of organically-bound sulphur in the geosphere: state of the art and future research.

907   *Organic Geochemistry*, **16** (4-6), 1077-1101.

908   SINNINGHE-DAMSTÉ, J. S., EGLINTON, T. I., RIJPSTRA, W. I. C. and DE LEEUW, J. W. 1990.

909   Molecular characterization of organically-bound sulphur in high-molecular-weight sedimentary

910   organic matter using flash pyrolysis and Raney Ni desulfurisation. *In* W. L. Orr and C. M. White

911   (eds). *Geochemistry of Sulfur in Fossil Fuels.* ACS symposium series, **429**, 486-528.

912   SINNINGHE-DAMSTÉ, J. S., EGLINTON, T. I., DE LEEUW, J. W. and SCHENCK, P. 1989. Organic

913   sulphur in macromolecular sedimentary organic matter: I. Structure and origin of sulphur-

914   containing moieties in kerogen, asphaltenes and coal as revealed by flash pyrolysis. *Geochimica*

915   *et Cosmochimica Acta*, **53** (4), 873-889.

916   SINNINGHE-DAMSTÉ, J. S., IRENE, W., RIJPSTRA, C., DE LEEUW, J. W. and SCHENCK, P.

917   1988. Origin of organic sulphur compounds and sulphur-containing high molecular weight

918   substances in sediments and immature crude oils. *Organic Geochemistry*, **13** (4-6), 593-606.

919   SLATER, T. S., MCNAMARA, M. E., ORR, P. J., FOLEY, T. B., ITO, S. and WAKAMATSU, K.

920   2020. Taphonomic experiments resolve controls on the preservation of melanosomes and

921   keratinous tissues in feathers. *Palaeontology*, **63** (1), 103-115.STANKIEWICZ, B., BRIGGS, D.

922   E. G., MICHELS, R., COLLINSON, M., FLANNERY, M. and EVERSHED, R. 2000.

923   Alternative origin of aliphatic polymer in kerogen. *Geology*, **28** (6), 559-562.

924   STANKIEWICZ, B., SCOTT, A., COLLINSON, M. E., FINCH, P., MÖSLE, B., BRIGGS, D. and

925   EVERSHED, R. 1998. Molecular taphonomy of arthropod and plant cuticles from the

926   Carboniferous of North America: implications for the origin of kerogen. *Journal of the*

927   *Geological Society*, **155** (3), 453-462.

928   STAROŃ, P., BANACH, M. and KOWALSKI, Z. 2011. Keratyna: źródła, właściwości, zastosowanie.

929   *Chemik*, **65** (10), 1019-1026.

930   STĘPIEŃ, K., DZIERŻĘGA-LĘCZNAR, A., KURKIEWICZ, S. and TAM, I. 2009. Melanin from

931   epidermal human melanocytes: study by pyrolytic GC/MS. *Journal of the American Society for*

932   *Mass Spectrometry*, **20** (3), 464-468

933 SULLIVAN, C., WANG, Y., HONE, D. W., WANG, Y., XU, X. and ZHANG, F. 2014. The vertebrates

934   of the Jurassic Daohugou Biota of northeastern China. *Journal of Vertebrate Paleontology*, **34**

935   (2), 243-280.

936 TEGELAAR, E. W., DE LEEUW, J. W., DERENNE, S. and LARGEAU, C. 1989. A reappraisal of

937   kerogen formation. *Geochimica et Cosmochimica Acta*, **53** (11), 3103-3106.

938 TEMPLIER, J., GALLOIS, N. and DERENNE, S. 2013. Analytical TMAH pyrolysis of dipeptides:

939   Formation of new complex cyclic compounds related to the presence of the peptide bond.

940   *Journal of Analytical and Applied Pyrolysis*, **104**, 684-694.

941 WANG, Y. X. and CAO, X. J. 2012. Extracting keratin from chicken feathers by using a hydrophobic

942   ionic liquid. *Process Biochemistry*, **47**, 896-899.

943 WANG, B., ZHAO, F., ZHANG, H., FANG, Y. and ZHENG, D. 2012. Widespread pyritization of

944   insects in the Early Cretaceous Jehol Biota. *Palaios*, **27** (10), 708-712.

945 WIEMANN, J., FABBRI, M., YANG, T. R., STEIN, K., SANDER, P. M., NORELL, M. A. and

946   BRIGGS, D. E. 2018. Fossilization transforms vertebrate hard tissue proteins into N-heterocyclic

947   polymers. *Nature communications*, **9** (1), 4741.

948 WILBY, P. R., BRIGGS, D. E. G. and RIOU, B. 1996. Mineralization of soft-bodied invertebrates in a

949   Jurassic metalliferous deposit. *Geology*, **24** (9), 847-850.

950 WOGELIUS, R., MANNING, P., BARDEN, H., EDWARDS, N., WEBB, S., SELLERS, W.,

951   TAYLOR, K., LARSON, P., DODSON, P. and YOU, H. 2011. Trace metals as biomarkers for

952   eumelanin pigment in the fossil record. *Science*, **333** (6049), 1622-1626.

953 WOJCIECHOWSKA, E., ROM, M., WŁOCHOWICZ, A., WYSOCKI, M. and WESEŁUCHA-

954   BIRCZYŃSKA, A. 2004. The use of Fourier transform-infrared (FTIR) and Raman spectroscopy

955   (FTR) for the investigation of structural changes in wool fibre keratin after enzymatic

956   treatment. *Journal of Molecular Structure*, **704** (1-3), 315-321.

957 XING, L., MCKELLAR, R. C., XU, X., LI, G., BAI, M., PERSONS, W.S., MIYASHITA, T.,

958   BENTON, M. J., ZHANG, J. and WOLFE, A. P. 2016. A feathered dinosaur tail with primitive

959   plumage trapped in Mid-Cretaceous amber. *Current Biology*, **26** (24), 3352-3360.

960 XU, X., WANG, ZHANG, K., MA, Q., XING, L., SULLIVAN, C., HU, D., CHENG, S. and WANG, S.

961   2012. A gigantic feathered dinosaur from the Lower Cretaceous of China. *Nature*, **484** (7392),

962   92-95.

963 XU, X., WANG, X. L. and WU, X. C. 1999. A dromaeosaurid dinosaur with a filamentous integument

964   from the Yixian Formation of China. *Nature*, **401** (6750), 262-266.

965 XU, X., ZHAO, Q., NORELL, M., SULLIVAN, C., HONE, D., ERICKSON, G., WANG, X. L., HAN,

966   F. L. and GUO, Y. 2009. A new feathered maniraptoran dinosaur fossil that fills a morphological

967   gap in avian origin. *Chinese Science Bulletin*, **54** (3), 430-435.

968 XU, X., ZHENG, X., SULLIVAN, C., WANG, X., XING, L., WANG, Y. X., ZHANG, X.,

969   O'CONNOR, J. K., ZHANG, F. and PAN, Y. 2015. A bizarre Jurassic maniraptoran theropod

970   with preserved evidence of membranous wings. *Nature*, **521** (7550), 70-73.

971 YANG, J. H., WU, F. Y., SHAO, J. A., WILDE, S. A., XIE, L. W. and LIU, X. M. 2006. Constraints on

972   the timing of uplift of the Yanshan Fold and Thrust Belt, North China. *Earth and Planetary*

973   *Science Letters*, **246**, 336-352.

974 YOSHIMIZU, H. and ANDO, I. 1990. Conformational characterization of wool keratin and 5'-

975   (Carboxymethy1) kerateine in the solid state by ^{13}C CP/MAS NMR spectroscopy.

976   *Macromolecules*, **23**, 2908-2912.

977 YUAN, H., LIU, X., LIU, Y., GAO, S. and LING, W. 2005. Geochemistry and U-Pb zircon

978   geochronology of Late-Mesozoic lavas from Xishan, Beijing. *Science in China: Series D Earth*

979   *Sciences*, **49** (1), 50-67.

980 YU, P., MCKINNON, J. J., CHRISTENSEN, C. R. and CHRISTENSEN, D. A. 2004. Using

981   synchrotron-based FTIR microspectroscopy to reveal chemical features of feather protein

982   secondary structure: comparison with other feed protein sources. *Journal of agricultural and*

983   *food chemistry*, **52** (24), 7353-7361.

984 ZHANG, H., WANG, M. X. and LIU, X. M. 2008. Constraints on the upper boundary age of the

985   Tiaojishan Formation volcanic rocks in West-Liaoning –North Hebei by LA-ICP-MS dating.

986   *Chinese Science Bulletin*, **53** (22), 3574-3584.

987 ZHAO, T., HU, J., HU, L. and PAN, Y., 2020. Experimental maturation of feathers: implications for

988   interpretations of fossil feathers. *Palaios*, **35** (2), 67-76.

989 ZHENG, X. T., YOU, H. L., XU, X. and DONG, Z. M. 2009. An early Cretaceous heterodontosaurid

990   dinosaur with filamentous integumentary structures. *Nature*, **458**, 333-336.

991 ZHOU, Z., JIN, F. and WANG, Y. 2010. Vertebrate assemblages from the Middle-Late Jurassic Yanliao

992   Biota in northeast China. *Earth Science Frontier*s, **17**, 252-254.

993 ZHU, M., BABCOCK, L. E. and STEINER, M. 2005. Fossilization modes in the Chengjiang Lagerstätte

994   (Cambrian of China): testing the roles of organic preservation and diagenetic alteration in

995   exceptional preservation. *Palaeogeography, Palaeoclimatology, Palaeoecology*, **220**, 31-46.

996

997 **FIGURE CAPTIONS**

998   Figure 1. *Anchiornis huxleyi* (YFGP-T5199). Photograph of the Jurassic feathered theropod with

999   location of sampled areas. The white box indicates locations of fossil feather and 'host' sediment

1000   sampling, while the yellow box indicates location of 'remote' sediment sampling, for NMR, Py-GC-MS,

1001   and IBA analyses. White dots are samples used for SEM imaging and EDS. Scale bar = 5 cm.

1002   Photograph by Thierry Hubin (IRSNB).

1003   Figure 2. Scanning electron microscopy (SEM) images of minerals observed in the plumage of

1004   *Anchiornis huxleyi*. (A), (B) thin platelets of phyllosilicates observed in sample 7 (see Fig. 1 for

1005   location); scale bar = 5 µm (A) and 3 µm (B), (C) Pyrite framboids (sample 1); scale bar = 10 µm, (D)

1006   Pyrite crystallites (sample 1); scale bar = 5 µm, (E) Clayed pores containing small star-shaped iron-

1007   oxide crystals (sample 8); scale bar = 2 µm, (F) Star-shaped iron oxides (sample 1); scale bar = 2 µm,

1008   (G) Feldspar crystal surrounded by clay sheets (sample 5); scale bar = 5 µm, (H) Quartz crystals

1009   embedded in a clayed matrix (sample 9); scale bar = 5 µm. Arrowheads point towards the

1010   aforementioned minerals. Abbreviations: Phy: phyllosilicate; Py: pyrite; Fd: feldspar; Qz: quartz.

1011   Figure 3. X-ray powder diffraction patterns of the 'host' sediment. Spectrum of (A) the bulk rock; qz,

1012   quartz; ca, calcite, (B) the fraction < 2 µm, with spectra of natural (N), glycolated (G), and heated (H)

1013   sample. The expansive illite/smectite interstratifications are identified in the spectrum of the glycolated

1014   (G) material.

1015   Figure 4. SEM images of the ultrastructure of *Anchiornis* plumage. (A), (B) elongated microbodies

1016   observed in sample 6 (see Fig. 1 for location), (C) Elongated microbodies (arrows) observed in sample

1017   9, and (D) imprints observed in samples 6. Scale bars: 2 µm.

1018   Figure 5. Results of Elastic Backscattering Spectrometry (EBS) and Particle-Induced X-ray Emission

1019   (PIXE) analyses on the fossil feathers, the 'host' sediment and the 'remote' sediment. (A) Global content

1020   of C, O and Si obtained by EBS, in integrating the C, O and Si depth profiles over the 0 – 25 000 TFU

1021   interval. The error bars give an estimate of the uncertainties considering the counting statistics as well as

1022   the cross-section and stopping power uncertainties. Analysis have been performed in duplicate on the

1023   same area of the fossil feather (Fossil #1, Fossil #2), three points of analysis have been taken at three

1024   different locations in the 'host' sediment (at 1.7, 3.2, and 4.8 mm away from the fossil), and one in the

1025   remote sediment (B) PIXE spectra obtained for one point of analysis in the fossil feather (red), the 'host'

1026   sediment (black), and the remote sediment (blue). The spectra are normalized to the Al signal (which is

1027   mainly coming from the selective filter) to allow for a direct comparison.

1028   Figure 6. Cross polarization/magic angle spinning ^{13}C nuclear magnetic resonance (CP-MAS ^{13}C-NMR)

1029   spectra of (A) the modern bird feather, (B) the fossil feathers, and (C) the 'host' sediment. Major

1030   chemical functions are indicated on each peak.

1031   Figure 7. IR spectra showing the comparison between of (A) a modern buzzard feather and *Anchiornis*

1032   feathers, and (B) *Anchiornis* feathers and the sedimentary matrix ('remote' sediment). See the text for

1033   peak assignment. The spectra are normalized to 100 % transmittance.

1034   Figure 8. Chromatograms of the products formed during the pyrolysis of (A) modern buzzard feathers,

1035   (B) fossil feathers, and (C) remote sediment. Peak identifications are given in Tables 2 and 3. C_n: carbon

1036   chain, with *n* indicating the length of the chain.

1037   Table 1. Sulphur content derived from PIXE using GUPIX for the data reduction. The global uncertainty

1038   is obtained by combining the counting statistics and the fit error (both calculated by GUPIX) with the

1039   estimated accuracy of our PIXE measurements. The latest contribution is obtained by direct comparison

1040   to a BCR-126A certified reference material. The global uncertainty is obtained by summing these three

1041   contributions in quadrature.

1042   Table 2. Significance of the peaks observed on the pyrochromatogram of the modern bird feather. Peaks

1043   are listed by increasing retention times. The table shows the complete name of each identified

1044   compound, the origin of these compounds, and whether they are observed in the modern feather, the

1045   fossil plumage, and the sediment. Peaks 1-18 and a-e were observed in the spectrum of the modern

1046   feathers, peaks f-g were observed in the spectrum of the fossil feather.

1047

Appendix

Molecular structures of compounds identified in the modern bird feathers. The correspondence with the numbers appears in Table 2

and Figure 8.

1051

1052

1053

1054

1055

1056

1057

1058

1059

1060

1061

1062

1063

1064

1065

1066   1   2   3   4

1067

1068

1069   5   6   7   8
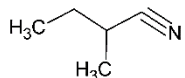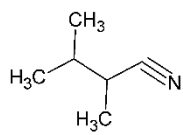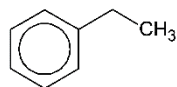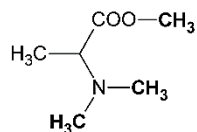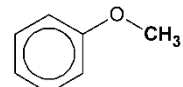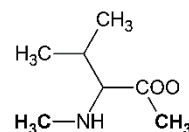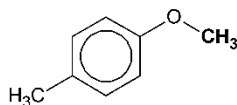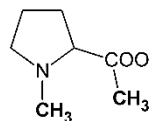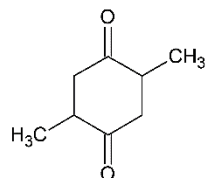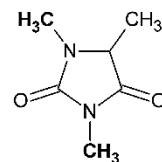
1070

1071

1072   9   10   11   12

1073
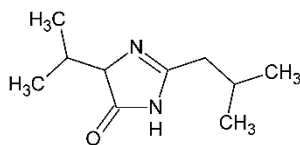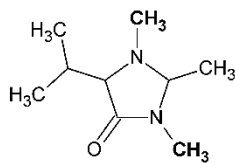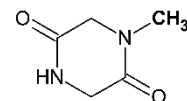
1074   13   14   15

1075
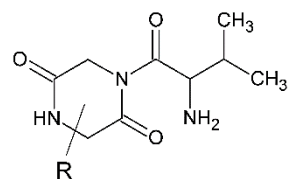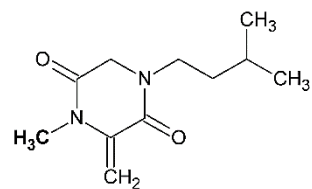
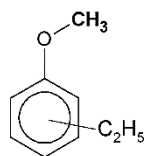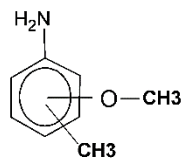1076   18   19   20,21

       22   23

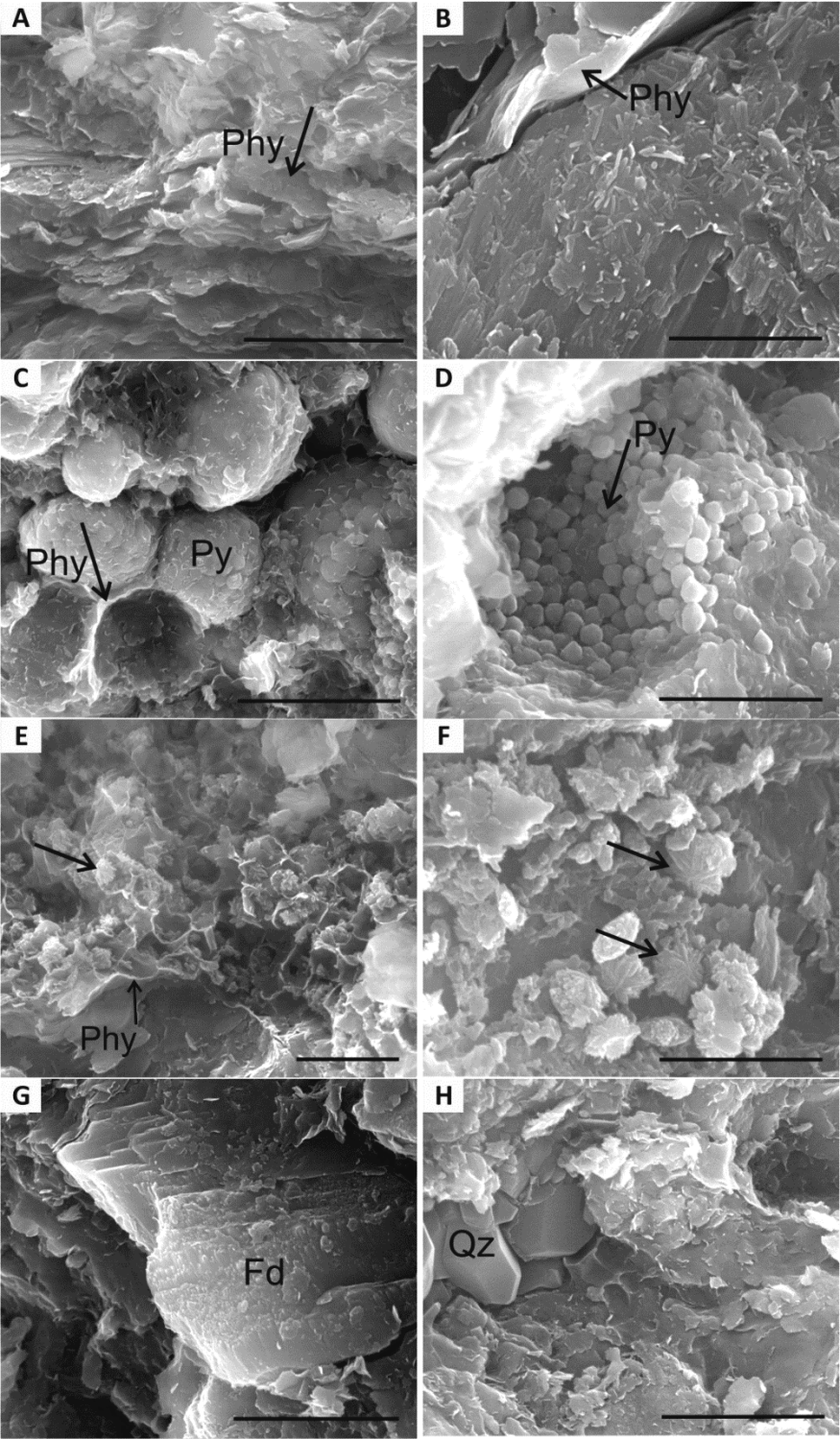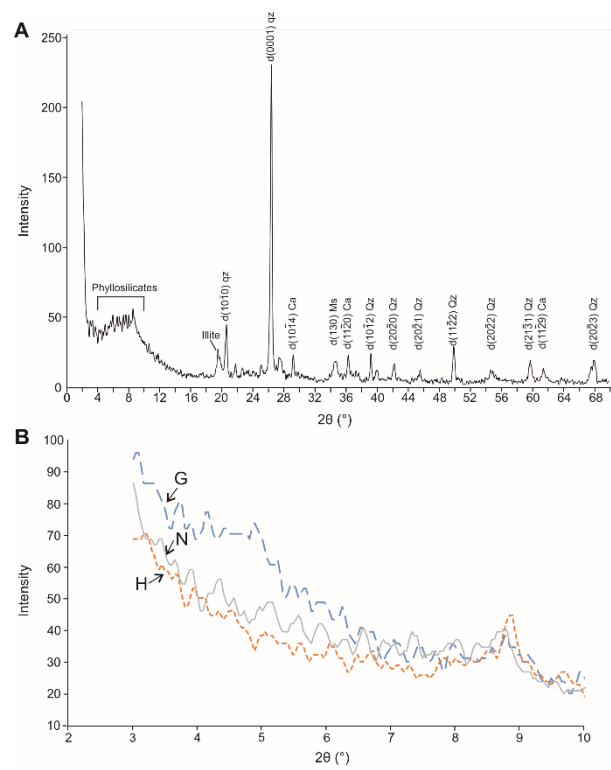1077
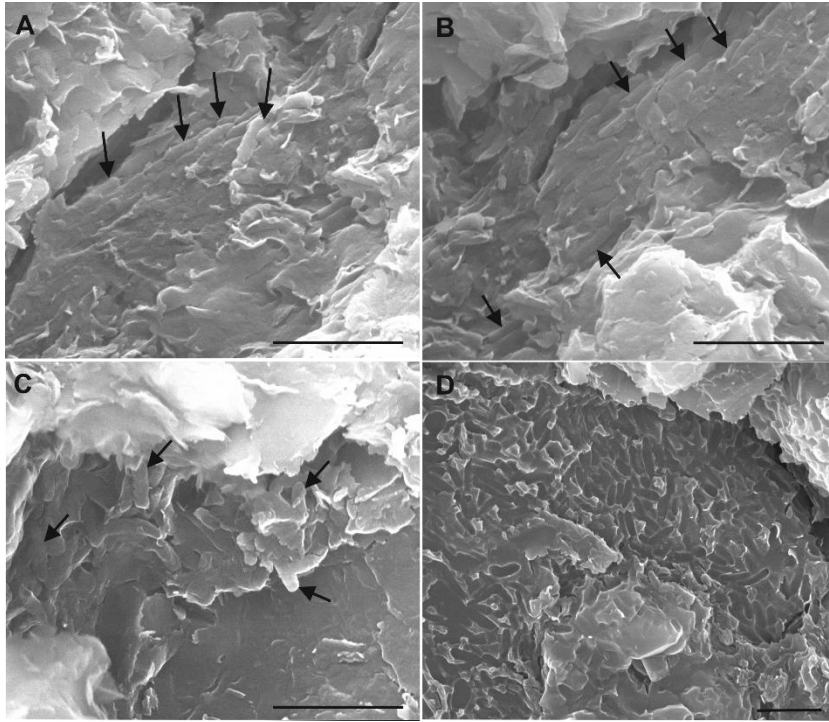
1078

1079

1080

1081

1082

1083

1084

1085

1086
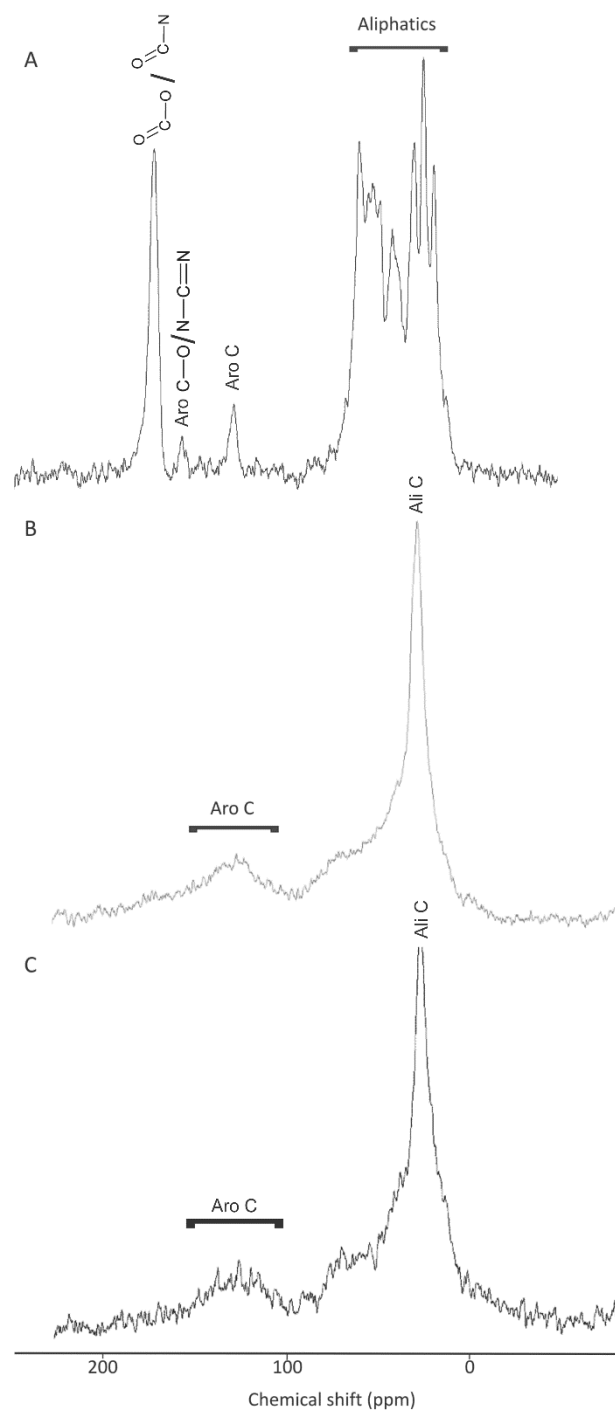
1087

1088

1089

1090

1091

1092

1093

58

1094

Legend:
- ● *n*-alkanes
- ○ *n*-alkenes
- △ fatty acid methyl esters
- □ alkyl benzenes
- ∗ TMAH and column phase derivatives

(A) Recent feathers

(B) Dinosaur feathers *A. huxleyi*

(C) Remote sediment

Y-axis: Relative abundance

X-axis: Retention time (min)
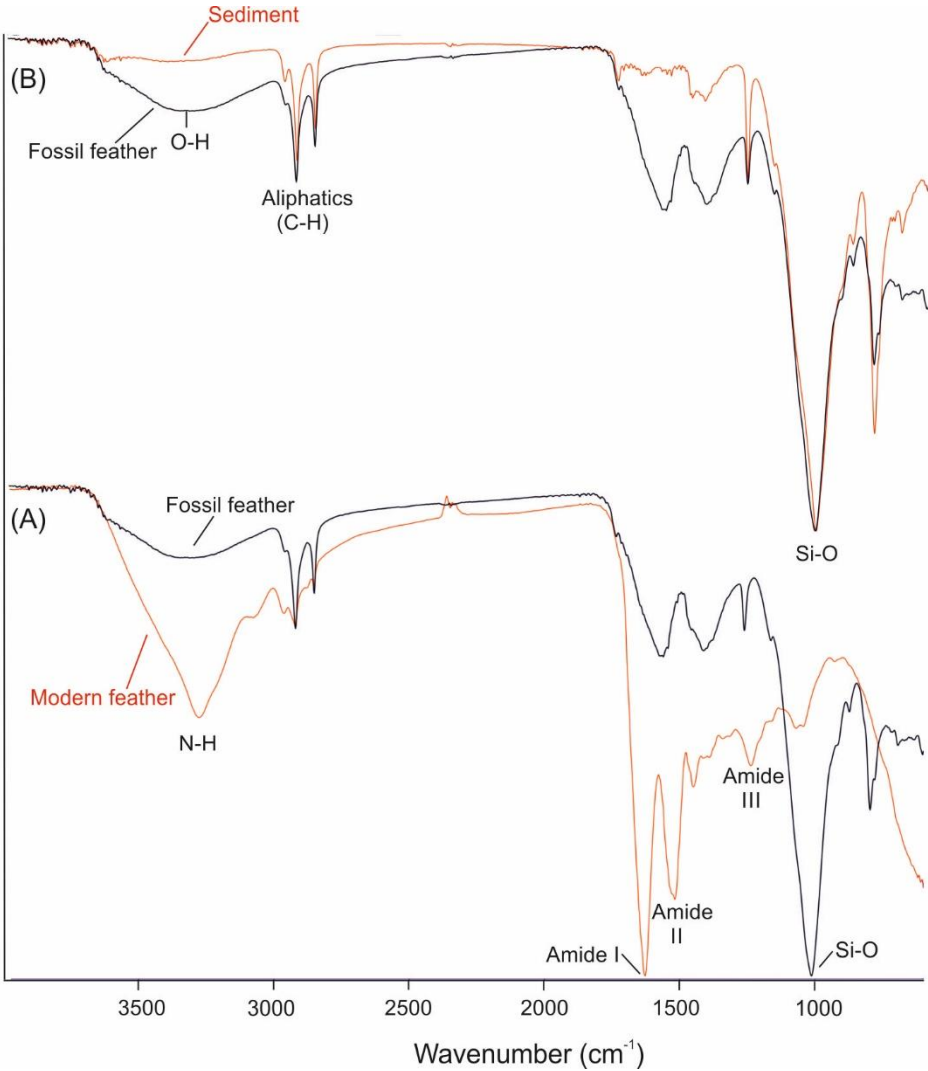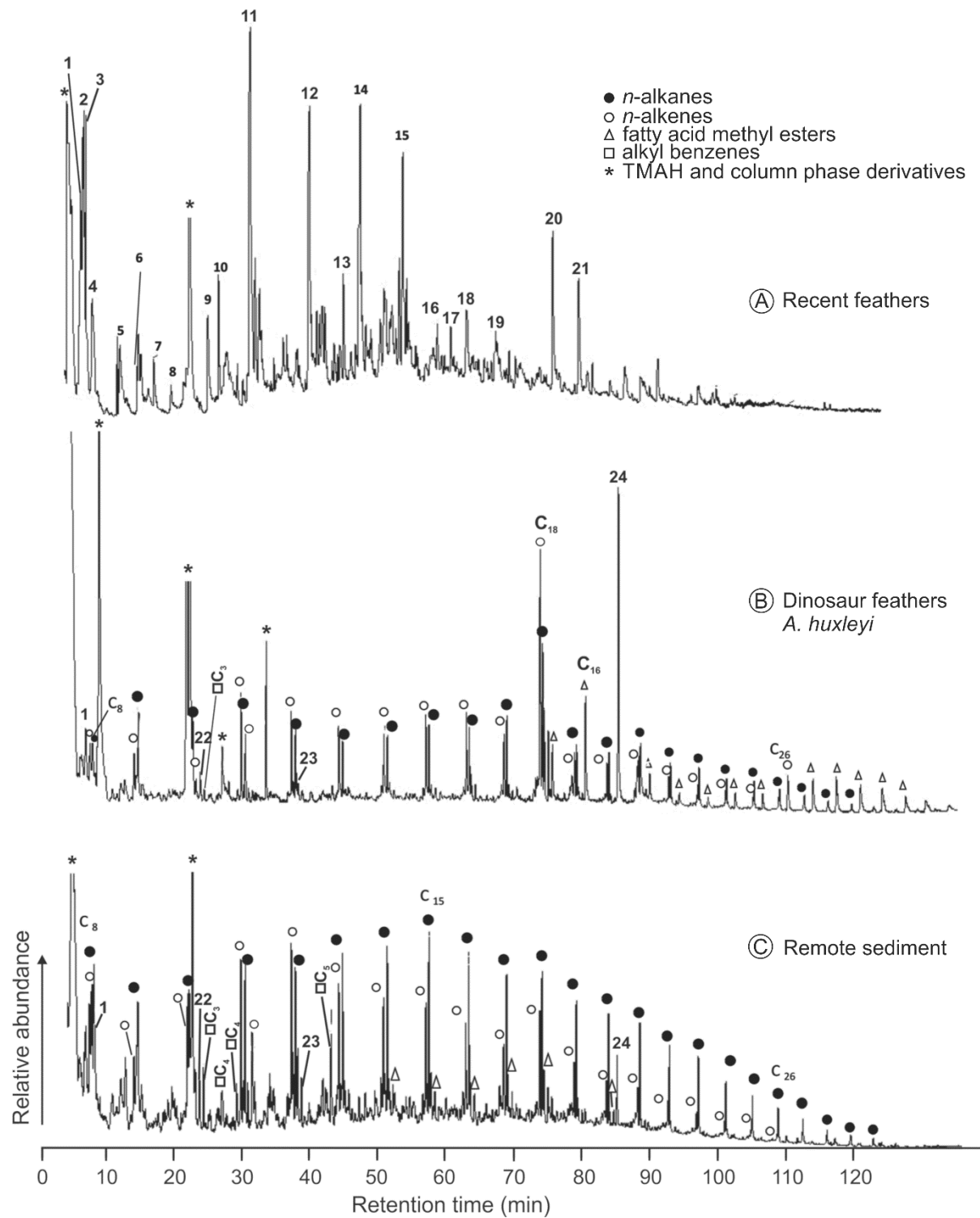
Table 1. PIXE derived concentration data for S and C in the fossil and modern feathers, and "host" sediment. The numbers in the left row represent the distance of the analyzed spots, away from the feather/sediment boundary. See Supplementary Table 1 for details on the global uncertainty calculations, Figure 1 and Supplementary Figure 2 for the location of the analyses.

	[S] (ppm)	[C] (ppm)
Fossil Feather #1	1739	80,385
Fossil Feather #2	1946	82,171
+1.7 mm	1162	72,012
+3.2 mm	801	49,213
+4.8 mm	893	41,835
Remote sediment	98	20,331
Rachis	37,142	547,174
Barbs	43,070	314,962

1098

1099

1100

1101

Peak	Retention time (min)	Major characteristic ions[a] (m/z)	Mole-cular ion	Compound	Possible origin[b]	Modern feather	Fossil feather[c]	Embedding sediment[c]
1	6.7	91; 92; 39; 65	92	Methylbenzene	(Phe)	X	X	X
2	6.9	55, 54, 42	83	2-methylbutanenitrile	Ileu	X		
3	7,1	43, 41, 39, 68	83	3-methylbutanenitrile	Leu	X		
4	8.0	67; 41; 39; 40	67	1H-Pyrrole	(Ser)	X		
5	12.1	91; 55; 106; 65	106	Ethylbenzene	(Phe)	X		
6	14.8	72; 42; 56; 131	131	N,N- Dimethylalanine methylester	Ala	X		
7	17.0	108; 78; 65; 39	108	Methoxybenzene	Tyr	X		
8	19.5	86; 102; 42; 55	145	N-Methyl-valine Methyl Ester	Val	X		
9	25.0	122; 77; 107; 91	122	1-Methoxy-4-methylbenzene	Tyr	X		
10	26.5	84; 42; 100; 58	143	N-Methyl-proline Methyl Ester	Pro	X		
11	31.2	56; 140; 42; 112; 83	140	2,5-Dimethylcyclohexane-1,4-Dione	Gly	X		
12	39.7	42; 127; 142; 56	142	1,3,5-Trimethylimidazolidine-2,4-Dione	Ala?	X		
13	44.8	56; 126; 139; 41	182	1-Isobutyl-4-isopropylimidazolinone	Val	X		
14	47.2	128; 42; 71; 113	170	5-Isopropyl-1,2,3-trimethylimidazolidinone	Val-(Gly)	X		
15	53.6	128; 42; 57; 71	128	1-Methylpiperazine-2,5-dione	Gly	X		
16	58.6	82; 167; 182; 110	182	?	His?	X		
17	60.5	152; 41; 55; 137; 179	194	?	Val?	X		
18	62.9	142; 113; 42; 71	198	1-Methyl-3-(1-methylpropyl)piperazine-2,5-dione	Ileu-Gly	X		
19	67.1	142; 113; 42; 98; 212	?	N-(1-oxo-2-amino-3-methyl-butyl)piperazine-2,5-dione derivative	Val	X		
20	75.5	139; 70; 42; 168	210	N-Methyl-3-methylidene-6-(3-methylbutyl)piperazine-2,5-dione	Ser-Leu	X		
21	79.2	168; 139; 70; 42	210	Isomer of compound 20	Ser-Leu	X		
22	23.7	136, 121, 122, 91	136	1-Methoxy-2,3-dimethylbenzene or 1-Ethyl-2-methoxybenzene	Lignin or cellulose		X	X
23	38.1	136, 122, 137	137	Methoxy-methylaniline	?		X	X
24	86.3	45; 57; 97; 224; 252	284	1-Methoxyoctadecane	?		X	X
●		43; 57; 71; 85		n-alkanes	Aliphatic chains		C_8-C_{30} (C_{18}, C_{11})	C_8-C_{29} (C_{15})
○		55; 43; 69; 83, 97		n-alk-1-enes	Aliphatic chains		C_8-C_{26} (C_{11}, C_{18})	C_8-C_{29} (C_{11}, C_{18})
Δ		87; 74; 43; 55		Fatty acid methyl esters	Aliphatic chains		C_8-C_{30} (C_{16})	C_8-C_{30} (C_{16})
□		91, 105		Alkyl benzenes	?		C_3	C_3-C_5 (C_5)

1102   Table 2. Main products released from pyrolysis of modern feathers, fossil feathers and embedding sediment in the presence of TMAH.

1103   [a] MS fragments are in order of decreasing abundance, with base peak underlined.

63

1104   [b] Compounds in brackets indicate possible origin that is not univocal; Ala, alanine; Gly, glycine; His, histidine; Phe, phenylalanine; Pro, proline;

1105   Ser, serine; Tyr, tyrosine; Val, valine; ? Tentative origin

1106   [c] C_{range} (C_{max}, C_{submax})

1107

1108

1109